Investigating the Reduction of Fluoroethylene Carbonate and Vinylene Carbonate in Lithium-Ion Cells with Silicon-Graphite Anodes

Richard Stockhausen,[a] Lydia Gehrlein,[a] Thomas Bergfeldt,[a] Andreas Hofmann,[a] Freya Janina Müller,[a] Julia Maibach,[a] Katarzyna Hofmann,[b] Ronald Gordon,[a] and Anna Smith*[a]

The electrolyte additives fluoroethylene carbonate (FEC) and vinylene carbonate (VC) improve the lifetime of lithium-ion batteries with silicon-containing anodes by their reduction yielding a more stable solid electrolyte interphase (SEI). However, the reductive decomposition mechanism of FEC and VC has not yet been fully clarified. For this purpose, we investigate the electrolyte decomposition in $LiNi_{0.6}Co_{0.2}Mn_{0.2}O_2$ (NCM622)/silicon-graphite pouch cells containing either 1 M $LiPF_6$ in FEC:dimethyl carbonate (DMC) or 1 M $LiPF_6$ in VC:DMC using high-performance liquid chromatography, gas chromatography, X-ray photoelectron spectroscopy, and inductively coupled plasma optical emission spectrometry. Based on the molar consumptions of FEC and VC, and the cumulative irreversible capacities, we show that three electrons are consumed for every reduced FEC molecule, and that one electron is consumed for every reduced VC molecule. Based on the results, reactions of the FEC reduction are proposed yielding LiF, Li_2CO_3, $Li_2C_2O_4$, HCO_2Li, and a PEO-type polymer. Furthermore, the reaction of the VC reduction is proposed yielding lithium-containing, polymerized VC. During formation, the capacity loss of the cells is induced by lithium trapping in Li_xSi_y/Li_xSiO_y under the SEI and by lithium trapping in the SEI. During subsequent cycling, only lithium trapping in the SEI triggers the capacity loss.

Introduction

Silicon represents a promising anode active material for future lithium-ion battery cells with improved energy density due to its high theoretical specific capacity (about 3600 $mAh \cdot g^{-1}$ regarding the phase $Li_{15}Si_4$),[1–3] which is about ten times higher than the theoretical specific capacity of the commonly used anode active material graphite (372 $mAh\,g^{-1}$).[4,5] Additionally, silicon is an abundant element on earth and has a low working potential of about 0.2 V vs. Li/Li^+, which also makes silicon an attractive anode active material for future lithium-ion battery cells with improved energy density.[6] However, the lithiation of silicon is accompanied by a strong volume increase of up to 320 % resulting in massive volume changes of the silicon during de-/lithiation.[7] As a result, new electrochemically active surface is created during cycling, which leads to ongoing solid electrolyte interphase (SEI) formation, continuous electrolyte consumption, and rapid irreversible capacity loss of the cell.[8] The lifetime of lithium-ion battery cells with silicon-containing anodes must be improved for a commercial application. One possibility to improve the electrochemical performance of such lithium-ion battery cells is to use a blend of a carbonaceous material, like graphite, and a silicon material as anode active material.[6,9] According to literature, the capacity loss of cells with silicon-graphite anodes is mainly induced by morphology changes of the silicon particles (such as pulverization) due to their large volume changes upon de-/lithiation during the initial cycles.[6] These morphology changes lead to massive SEI growth on the silicon, which is associated with fast capacity loss and disruption of the electrical connection between the anode materials.[6] After the initial cycles, the mechanical stress by the volume changes is reduced in the pulverized silicon particles, so that their morphology have reached a steady state and the silicon particle pulverization is stopped or decelerated.[6] The initial silicon particle pulverization yields smaller silicon particles, whose diameters are below the critical threshold (150 nm), so that the particles remain resistant to further pulverization.[10] However, the mechanical stress in the pulverized silicon particles is still sufficient to damage the SEI, which leads to further SEI growth and thus to a slow capacity loss after the initial cycles during long-term cycling.[6] In large-scale commercial cells with a low electrolyte to active material mass ratio, the electrolyte consumption due to the SEI growth and

[a] *R. Stockhausen, L. Gehrlein, T. Bergfeldt, A. Hofmann, F. Janina Müller, J. Maibach, R. Gordon, A. Smith*
Karlsruhe Institute of Technology (KIT), Institute for Applied Materials (IAM), Hermann-von-Helmholtz-Platz 1, 76344 Eggenstein-Leopoldshafen, Germany
+49 721 608–28851
+49 721 608–28284
E-mail: anna.smith@kit.edu

[b] *K. Hofmann*
Karlsruhe Institute of Technology (KIT), Institute of Mechanical Process Engineering and Mechanics, Straße am Forum 8, 76131 Karlsruhe, Germany

the pore volume increase due to the silicon particle pulverization can lead to a partial dry-out of the silicon-graphite anode and thus to a sudden capacity drop.[6] Meanwhile, the graphite is not covered by a thick SEI in cells with silicon-graphite anodes due to its low volume change during de-/lithiation (< 10 %).[6] Beside the use of silicon-graphite composite anodes, another promising possibility to improve the lifetime of lithium-ion battery cells with silicon-containing anodes is the use of electrolyte additives.[11] It is already known that specific electrolyte additives can form a flexible SEI on silicon, which survives the massive volume changes of the silicon during de-/lithiation without the creation of new electrochemically active surface, whereby an improved cycling stability is enabled.[11] Fluoroethylene carbonate (FEC) and vinylene carbonate (VC), for instance, are the most frequently used SEI-forming electrolyte additives to enhance the lifetime of lithium-ion batteries.[11] Nowadays, FEC is a standard electrolyte additive for lithium-ion battery cells with silicon electrodes due to the significant improvement of the cycling stability by FEC.[8] Generally, VC is the most commonly used and most studied electrolyte additive for lithium-ion battery cells.[12] VC is sometimes used as additive also for lithium-ion cells with silicon anodes.[11] However, the mechanisms for the reductive decomposition of FEC and VC in lithium-ion cells have not yet been fully clarified. For this purpose, the decomposition products from FEC and VC, as well as the number of consumed electrons per consumed FEC molecule or VC molecule should be determined. Usually, only the decomposition products from FEC and VC, namely the resulting SEI components and the evolved gases, are investigated. The corresponding number of consumed electrons per consumed FEC or VC molecule, however, reveals whether FEC or VC is reduced via a 1-electron reduction, a 2-electron reduction, or a 3-electron reduction, and so on. Admittedly, the number of consumed electrons per reduced FEC molecule has already been determined in few studies.[8,13,14] However, these reports are partially contradictory: Jung et al. and Solchenbach et al. found that four electrons are consumed for each reduced FEC molecule,[8,13] while Wetjen et al. found that three electrons are consumed for each reduced FEC molecule.[14] The number of consumed electrons per reduced VC molecule have never been experimentally determined to the best of our knowledge. Furthermore, mainly half-cells with a silicon-containing electrode and a lithium metal counter electrode or full-cells with a silicon-containing anode and a capacitively oversized cathode have been investigated.[8,14–20] In a conventional full-cell configuration with a capacitively oversized anode, the amount of cycleable lithium is limited by the capacity of the cathode.[21] Consequently, the loss of cycleable lithium due to the SEI formation/growth on the anode translates directly into a capacity loss of the battery cell.[21] In half-cells or full-cells with a capacitively oversized cathode, this loss of cycleable lithium is recovered from the lithium metal counter electrode or the cathode, so that it does not appear as capacity loss of the cell.[21] As a result, the mechanisms responsible for capacity loss of conventional full-cells with a capacitively oversized anode differ from the mechanisms responsible for capacity loss of half-cells or full-cells with a capacitively oversized cathode. Additionally, in the published studies, coin cells with silicon-containing electrodes are usually examined, in which the electrolyte volume is excessive compared to the active mass of the electrodes.[21] However, it is important to study silicon-based electrodes in a full-cell configuration with a relatively low electrolyte to active material mass ratio, such as pouch cells, that is close to the electrolyte to active material mass ratio in commercial cells.[21] Summarized, there are only few studies, in which the capacity loss mechanisms of conventional full pouch cells with capacitively oversized, silicon-containing anodes are investigated.[21]

To further fill this research gap, in this work we investigate the mechanisms responsible for the capacity loss of NCM622/silicon-graphite lithium-ion pouch cells, which contain either the electrolyte 1 M $LiPF_6$ in FEC:dimethyl carbonate (DMC) 1 : 1 by weight or the electrolyte 1 M $LiPF_6$ in VC:DMC 1 : 1 by weight. Thereby, new insights into the reductive decomposition of FEC and VC are also gained. The electrolytes are extracted from these pouch cells before formation and after different numbers of cycles. The extracted electrolytes are quantitatively analyzed by high-performance liquid chromatography (HPLC) coupled to an electrospray ionization mass spectrometer (ESI/MS) and an ultraviolet/visible light (UV/Vis) detector, as well as by gas chromatography (GC) coupled to a flame ionization detector (FID) to determine the consumptions of the electrolyte components in the cells upon formation and subsequent cycling. The applied electrolyte extraction method and the determination of the consumptions of the electrolyte components in the battery cells was already used for the investigation of the electrochemical electrolyte decomposition in $LiNi_{1/3}Co_{1/3}Mn_{1/3}O_2$ (NCM111)/graphite pouch cells[22] and NCM622/graphite pouch cells.[23] Based on the electron consumption at the anodes (calculated by means of the cumulative irreversible capacity) and the FEC or VC consumption, the number of consumed electrons per reduced FEC or VC molecule is calculated. For the determination of the number of consumed electrons per reduced FEC or VC molecule, it should be ensured that FEC or VC is only reduced at one electrode. In case of a half-cell with a silicon-containing working electrode, SEI-forming additives like FEC (or VC) are reduced not only at the working electrode but also at the lithium metal counter electrode.[8] As a result, electrons, as well as FEC (or VC) molecules are consumed at both electrodes,[8] which makes the determination of the number of consumed electrons per reduced FEC (or VC) molecule more complex. In contrast, SEI-forming additives like FEC (or VC) are only reduced at the silicon-containing anode in a full-cell,[8] which simplifies the determination of the number of consumed electrons per reduced FEC (or VC) molecule. For that reason, full-cells are also used for the determination of the number of consumed electrons per reduced FEC or VC molecule in this study. To identify the products from the reductive decomposition of FEC and VC, and to determine the triggers for the capacity losses of the cells, complementary analysis methods are applied. Based on the results from the analyses of the pouch cells, reactions of the reductive decomposition of FEC and VC are proposed. Moreover, the triggers for the capacity losses of the examined

NCM622/silicon-graphite pouch cells during formation and during subsequent cycling are identified. The results of this study have already been published in more detail in a doctoral thesis.[24]

Experimental

Cell Components

For the examined NCM622/silicon-graphite pouch cells, custom-made electrodes were utilized. The one-sided coated silicon-graphite anodes from the pouch cells had dimensions of 5.2×5.2 cm. The anode coating consisted of 84.15 wt% graphite (SMG-A5, Hitachi, Japan), 9.35 wt% silicon nanopowder (average particle size: 30–50 nm, purity: >98%, Nanostructured & Amorphous Materials, USA), 1.9 wt% carbon black (Timcal C65, Imerys, France), 1.75 wt% sodium carboxymethylcellulose (NaCMC) binder (CRT 2000 PA 07, $M_w = 150$ kDa, degree of substitution: 0.7, DuPont, USA), and 2.85 wt% styrene-butadiene rubber (SBR) binder (TRD 2001, JSR, Japan). This anode coating was applied onto copper foil with a mass loading of 4.6 mg cm^{-2}. The theoretical areal capacity of these anodes was 3.0 mAh cm^{-2}. The dimensions of the one-sided coated NCM622 cathodes from the pouch cells were 5.0×5.0 cm. The cathode coating was composed of 94 wt% NCM622 (Targray, Canada), 3 wt% polyvinylidene fluoride (PVDF) binder (Solef 5130, Solvay, Belgium), 1 wt% carbon black (Super C65, Imerys, France), and 2 wt% graphite (Timcal SFG6 L, Imerys, France). This cathode coating was applied onto aluminum foil with a mass loading of 10.8 mg cm^{-2}. The theoretical areal capacity of these cathodes was 1.8 mAh cm^{-2}. The theoretical areal capacity of the anodes was distinctly higher than the theoretical areal capacity of the cathodes to prevent lithium plating during cycling. The separators used for the pouch cells were PET-based and ceramically coated with dimensions of 5.5×5.5 cm. Before the assembly of the pouch cells, the electrodes and separators were dried under reduced pressure for 12 h at 130 °C and 180 °C, respectively.

The electrolytes were mixed in an argon-filled glovebox (oxygen and water content <1 ppm). The added electrolyte components were weighed to determine the precise initial electrolyte compositions. The water content of the electrolytes was less than 20 ppm, which was determined by Karl Fischer titration. The assembled NCM622/silicon-graphite pouch cells were filled either with the electrolyte 1 M $LiPF_6$ in FEC:DMC or 1 M $LiPF_6$ in VC:DMC, whose compositions are listed in Table 1. DMC (anhydrous, ≥99%) and $LiPF_6$ (battery grade, ≥99.99%) were purchased from Sigma-Aldrich (USA). FEC (≤20 ppm water, ≥99.5%) and VC (≤200 ppm water, ≥99.5%) were purchased from Gotion (USA).

To check whether electronically connected active material was lost during cycling, the areal capacities of electrodes from NCM622/silicon-graphite pouch cells after formation and after 40 cycles were determined by means of coin cells (half-cells). The working electrodes from these assembled half-cells were punched out of silicon-graphite anodes and NCM622 cathodes from the disassembled NCM622/silicon-graphite pouch cells. The diameter of the punched silicon-graphite electrodes was 13 mm, whereas the diameter of the punched NCM622 electrodes was 12 mm. The counter electrode from the assembled coin cells consisted of lithium metal (diameter: 15 mm, thickness: 1.5 mm, 99.9%, Sigma-Aldrich, USA). Whatman glass fiber filters (diameter: 17 mm, grade: GF/D, Cytiva, Germany) were used as separators in the assembled coin cells. The electrolyte 1 M $LiPF_6$ in FEC:DMC was filled into the coin cells with the working electrodes that were punched out of the electrodes from the pouch cells with the initial electrolyte 1 M $LiPF_6$ in FEC:DMC. The electrolyte 1 M $LiPF_6$ in VC:DMC was filled into the coin cells with the working electrodes that were punched out of the electrodes from the pouch cells with the initial electrolyte 1 M $LiPF_6$ in VC:DMC.

Cell Assembly

The pouch cells were assembled in a dry room with a dew point of −60 °C. In each pouch cell, two anodes were placed back to back in the middle, such that both anodes each faced one one-sided coated cathode. In addition, two separators were used in each pouch cell. 900 µl of the respective electrolyte (see Table I) was filled into each pouch cell. After electrolyte filling, the cells were sealed under reduced pressure. The weight of the pouch cell was determined before and after electrolyte filling and sealing to calculate the initial electrolyte mass within the pouch cell. The theoretical capacities of the pouch cells were approximately 85 mAh. The coin cells (half-cells) were assembled in an argon-filled glovebox (oxygen and water content <1 ppm). In each coin cell, a working electrode, a separator, and a lithium metal counter electrode were installed. The working electrodes were punched out of NCM622 cathodes and silicon-graphite anodes from disassembled NCM622/silicon-graphite pouch cells. Either 300 µl of the electrolyte 1 M $LiPF_6$ in FEC:DMC or 300 µl of the electrolyte 1 M $LiPF_6$ in VC:DMC was filled into the coin cell.

Cell Formation and Cycling

A Basytec CTS LAB was used for the formation and the cycling of the cells. For formation and cycling, the cells were placed in a climate chamber with a constant temperature of 25 ± 0.1 °C.

The formation program included two cycles: The pouch cells were first charged with 0.1 C to 4.2 V with constant current-constant voltage (CC–CV), until the current fell below 0.05 C (I < 0.05 C). Subsequently, the pouch cells were discharged with 0.1 C to 3.0 V with constant current (CC). Following this, the pouch cells were charged again with 0.5 C to 4.2 V (CC–CV, until I < 0.05 C) and discharged with 0.5 C to 3.0 V (CC). Thereafter, the formation program was finished for the pouch cells, which were further cycled after formation. The pouch cells that were investigated directly after their formation were held at 3.0 V for four hours after the discharge at 0.5 C before the analyses. Some pouch cells were cycled after formation for further 15 or 40 cycles in a voltage range of 3.0 V-4.2 V with charge at 0.5 C (CC–CV, until I < 0.05 C) and discharge at 0.5 C (CC). A checkup cycle was conducted, during which the pouch cells were charged at 0.1 C to 4.2 V (CC–CV, until I < 0.05 C) and discharged at 0.1 C to 3.0 V (CC) at the beginning (right before the

Table 1. Compositions of the initial electrolytes from the investigated pouch cells.

Electrolyte	Mass fraction of DMC [wt%]	Mass fraction of $LiPF_6$ [wt%]	Mass fraction of FEC [wt%]	Mass fraction of VC [wt%]
1 M $LiPF_6$ in FEC:DMC	44.2 ± 0.1	11.6 ± 0.1	44.2 ± 0.1	0.0
1 M $LiPF_6$ in VC:DMC	44.0 ± 0.1	12.0 ± 0.1	0.0	44.0 ± 0.1

first cycle of the 0.5 C/0.5 C cycling described above). Following the checkup cycle, the DC internal resistances were determined by means of discharge pulses with 1 C for 20 s at different states of charge (SOCs), namely 10 %, 30 %, 50 %, 70 %, and 90 %. The SOCs were set by charging with 0.1 C using the Ah-counter method. The DC internal resistances were determined by the potential drop during the discharge pulse and the applied current during the discharge pulses using Ohm's law. After the 0.5 C/0.5 C cycling and before the analyses, the pouch cells were finally charged with 0.1 C to 4.2 V (CC–CV, until $I < 0.05$ C), discharged with 0.1 C to 3.0 V (CC), and held at 3.0 V for four hours. For the pouch cells, the mentioned C-rates were referenced to the respective theoretical capacity of the cathodes.

The coin cells (half-cells) with the punched silicon-graphite electrodes were discharged with 0.1 C to 0.005 V (CC–CV, until $I < 0.05$ C) and charged with 0.1 C to 1.0 V (CC) for two times/cycles. The coin cells (half-cells) with the punched NCM622 electrodes were charged at 0.1 C to 4.3 V (CC–CV, until $I < 0.05$ C) and discharged at 0.1 C to 3.0 V (CC) for two times. For the coin cells, the C-rate was referenced to the respective theoretical capacity of the silicon-graphite electrode or the NCM622 electrode from the coin cell.

Electrolyte Extraction

The electrolytes were extracted from the pouch cells by injection of diethyl carbonate (DEC, anhydrous, $\geq$ 99 %, Sigma-Aldrich, USA) as diluent. This extraction method is described in detail in a previous publication.[22] Briefly, 1000 µl DEC was injected into each pouch cell by a syringe. Subsequently, the pouch cell was sealed again under reduced pressure. The pouch cell was weighed before and after the DEC injection to calculate the exact mass of the injected DEC. Afterwards, the pouch cell was stored for 14 days at room temperature to allow a complete mixing of the injected DEC with the original electrolyte in the pouch cell. Following this, the electrolyte was extracted through a puncture, filtered by a syringe filter (pore size: 0.1 µm), and diluted with acetonitrile (ACN). The DEC injection and the proper extraction were carried out in a dry room with a dew point of −60 °C.

HPLC Conditions and Sample Preparation for HPLC Analyses

For the quantification of DEC, DMC, and VC in the extracted electrolytes, a HPLC system of Nexera XR Ultra High Performance Liquid Chromatograph (Shimadzu, Japan) coupled to a type of UV/Vis detector, namely a photodiode array (PDA) detector (SPD–M20 A, Shimadzu, Japan) was used. To separate the electrolyte components, the column Acclaim 120 C18 (Thermo Fisher Scientific, USA) was used with the following characteristics: 250 mm length×4.6 mm interior diameter, particle size of 5 µm, and pore size of 120 Å. The temperature of the column oven temperature was constantly 50 °C during the measurements. The cell temperature of the PDA detector was set to 50 °C. The slit width of the PDA detector was 1.2 nm. The wavelength of the PDA detector was set to 190 nm. For the analyses, the flow rate was set to 1.00 ml min^{-1} and the injection volume to 2.0 µl. The mobile phase consisted constantly of 60 % water and 40 % ACN (isocratic separation) during the measurements. Each sample was injected three times, and the respective average peak area from these three measurements was used for the quantifications to minimize the statistical errors.

For the quantification of Li^+ and PF_6^- in the extracted electrolytes, the same HPLC system coupled to an ESI/MS (LCMS-2020, Shimadzu, Japan) was used. To separate the electrolyte components for the HPLC-ESI/MS analyses, the column Acclaim 120 C18 (Thermo Fisher Scientific, USA) was utilized with the following characteristics: 100 mm length×3.0 mm interior diameter, particle size of 2.2 µm, and pore size of 120 Å. During the HPLC-ESI/MS analyses, the temperature of the column oven was 50 °C, and the flow rate was 0.75 ml·min^{-1}. Furthermore, the injection volume was set to 1.0 µl. The composition of the mobile phase during HPLC-ESI/MS measurements is listed in Table T-S1 in the supplementary information. Additionally, the nebulizing gas flow was 1.5 l min^{-1}, whereas the drying gas flow was 20.0 l min^{-1}. Moreover, the heat block temperature was 400 °C, the desolvation line (DL) temperature was 300 °C, and the interface temperature was 350 °C during the HPLC-ESI/MS measurements. Each sample for the quantification of Li^+ and PF_6^- was injected four times. The respective average peak area from these four measurements was used for the quantifications of Li^+ and PF_6^- to minimize the statistical errors. PF_6^- was quantified by means of the PF_6^- peak itself in the trace of $m/z = 145.0^-$ u. Li^+ was quantified by means of the peak in the trace of $m/z = 89.1^+$ u. This peak can be attributed to a Li^+ linked with two ACN molecules ($Li^+ + 2$ ACN).[22]

The software LabSolutions Version 5.97 was used to control the system and to evaluate the data from the HPLC analyses.

For all the quantifications, the external standard method with a seven-point calibration was used. The extracted electrolytes and the standard substances were diluted with ACN. The ranges of the mass fractions of the analytes in the standard samples and the electrolyte-containing samples are listed in Table T-S2 in the supplementary information. The sample preparation for the HPLC analyses were conducted in a dry room with a dew point of −60 °C. Each mass was weighed during sample preparation for the quantifications.

GC Conditions

For the quantification of FEC in the extracted electrolytes, a Clarus 690 GC (PerkinElmer, USA) coupled to a FID was used. To separate the electrolyte components, an OPTIMA 5MS column (Macherey-Nagel, Germany) was used with the following characteristics: 30 m length×0.25 mm interior diameter and 0.5 µm film thickness. The injection volume was 0.5 µl, while the injector temperature was 250 °C. Helium gas 6.0 was used as carrier gas with an initial pressure of 220 kPa. The split flow for the injections was 20 ml min^{-1}. During the GC-FID measurements, the temperature of the column oved was changed as follows: Constantly 40 °C during the first 1.5 min, heating at 20 °C min^{-1} until a temperature of 220 °C, 5 min at a constant temperature of 220 °C, heating at 20 °C min^{-1} until a maximum temperature of 280 °C, 1.5 min at a constant temperature of 280 °C. The gas flows in the FID were 45 ml min^{-1} for hydrogen and 450 ml min^{-1} for synthetic air. The temperature of these gases was 250 °C during the analyses. Each sample was analyzed three times, and the respective average peak area from these three measurements was used for the quantifications of FEC. The external standard method with a nine-point calibration was used to quantify FEC. The ranges of the mass fractions of FEC in the standard samples and the electrolyte-containing samples are shown in Table T-S2 in the supplementary information.

To quantify the amounts of the evolved gases in the pouch cells, a Clarus 690-Arnel GC system (PerkinElmer, USA) equipped with two TCDs was used. The gases extracted from the pouch cells were injected into the gas injection system to fill all gas loops of the GC system with the extracted gases. For the analyses, either helium or nitrogen were used as carrier gases. The mentioned gases from the pouch cells were detected by the TCD-Arnel GC system.

For the control of the system and the evaluation of the data from the GC analyses, Turbomass 6.1.2 and TotalChrom 6.3.4 software packages were used.

Gas Extraction and Calculation of the Gas Amounts

A gas extraction valve was used to extract the gas from pouch cells. This gas extraction method is registered as patent[25] and enables not only the determination of the concentrations of the gases in the pouch cell, but also the determination of their amounts. For this purpose, pouch cells were assembled each with an integrated gas extraction valve, namely a double-end shutoff (DESO) Swagelok valve. To extract the gas, the gas extraction valve of the cell was connected to a gas loop that is equipped with a DESO Swagelok valve. The gas from the cell expanded into the gas loop after connection. Before and after connecting the cell, the pressure in the gas loop was determined. Subsequently, the extracted gas in the gas loop was injected into the gas injection system for the analyses by GC-TCD. Detailed information on the calculation of the absolute gas amounts can be found in section SI-3 of the supplementary information.

Calculation of the Consumptions of the Electrolyte Components

The calculation of the consumptions of the electrolyte components in the pouch cells is described in a previous publication[22] and a detailed description of the calculations is shown in section SI-4 of the supplementary information.

XPS Conditions and Sample Preparation for XPS Analyses

The XPS analyses were realized using a K-Alpha spectrometer (Thermo Fisher Scientific, UK). For the XPS analyses, a microfocused, monochromated Al K_α X-ray source was used with a spot size of 400 μm and a pass energy of 50 eV. For data acquisition and handling, the Thermo Avantage software by Parry et al. was used.[26] The spectra were fitted by one or more Voigt profiles. Scofield sensitivity factors were applied for the quantifications. All spectra were referenced in binding energy to the hydrocarbon peak at 285 eV in the C1s spectrum. The intensities of each spectrum were normalized to its maximum intensity.

Pouch cells were opened and anode pieces were cut for sample preparation. Afterwards, the cut anode pieces were briefly submerged in 1 ml DMC to remove the electrolyte. Subsequently, the anode pieces were mounted on a sample holder by a conductive copper tape. The sample preparation was carried out in an argon-filled glovebox (oxygen and water content < 1 ppm). For the transfer of the prepared samples to the spectrometer under inert gas conditions, a transfer module was used.

ICP-OES Conditions, Sample Preparation for ICP-OES Analyses, and Evaluation of the Measurement Data

To quantify lithium in electrodes from pouch cells, an iCAP 7600 ICP-OES Duo (Thermo Fisher Scientific, USA) was used. The lithium quantification was performed using four different matrix adapted standard samples and the internal standard scandium that was added to each sample with a mass fraction of about $2.00 \cdot 10^{-4}$ wt%. The three major wavelengths of lithium were used for the lithium quantifications. The ranges of the lithium mass fractions in the samples and the wavelengths used for the quantifications are indicated in the Tables T-S3 and T-S4 within section SI-5 in the supplementary information.

Pouch cells (except for the fresh cells) were discharged to 3 V and subsequently held at 3 V for four hours before the sample preparation for the ICP-OES measurements. The anodes and cathodes extracted from the pouch cells were submerged in DMC for one hour. Following this, the electrodes were air dried at room temperature for half an hour. For the calculation of the absolute lithium amounts in the electrodes, both anodes and both cathodes from each examined pouch cell were subsequently weighed. Pieces were subsequently cut out of these electrodes. The pieces of the anodes and cathodes with a total weight of about 40–70 mg per cell were weighed and submerged in aqua regia (composed of 6 ml hydrochloric acid subboiled and 2 ml nitric acid subboiled). The aqua regia with the electrode pieces was stored in a graphite oven at 80 °C for four hours. Detailed information about the calculation of the amount of lithium in the anodes and the lithium loss of the cathodes can be found in section SI-5 of the supplementary information.

Results and Discussion

In the following, the results of the different analyses of the electrolytes, the gases, and the electrodes from the investigated NCM622/silicon-graphite pouch cells are presented. Cells are examined in the electrochemically untreated fresh state, after formation, after 15 cycles, and after 40 cycles. These cells are initially filled with either the electrolyte 1 M $LiPF_6$ in FEC:DMC (called "cells with the FEC electrolyte") or the electrolyte 1 M $LiPF_6$ in VC:DMC (called "cells with the VC electrolyte"). Both electrolytes are selected because they are rich in FEC or VC, so that an exclusive reduction of FEC or VC can be expected, which enables the investigation of the reductive decomposition of FEC and VC without an interference by simultaneous decompositions of the other electrolyte components. Based on the results, reactions of the reductive decomposition of VC and FEC are proposed. In addition, the capacity loss mechanisms in the pouch cells are identified.

Capacities of the Pouch Cells

Figure 1a shows the absolute discharge capacities of NCM622/silicon-graphite pouch cells cycled at 0.5 C/0.5 C in dependence on the number of cycles. In Figure 1b, the associated relative discharge capacities of these cells are shown in dependence on the number of cycles.

The initial absolute discharge capacities from the cells with the FEC electrolyte are considerably higher than those from the cells with the VC electrolyte (see Figure 1a). This observation can be ascribed to the higher coulombic efficiencies of the first cycle of the formation from the cells with the FEC electrolyte (about 70%) compared to those from the cells with the VC electrolyte (about 64%). As a result, the irreversible capacity loss of the cells with the FEC electrolyte is lower than the irreversible capacity loss of the cells with the VC electrolyte during formation, which leads to this observation. Admittedly, the initial discharge capacities of the cells (see Figure 1a) are distinctly lower than the theoretical discharge capacity of the cells (about 85 mAh). The strong SEI formation especially on the

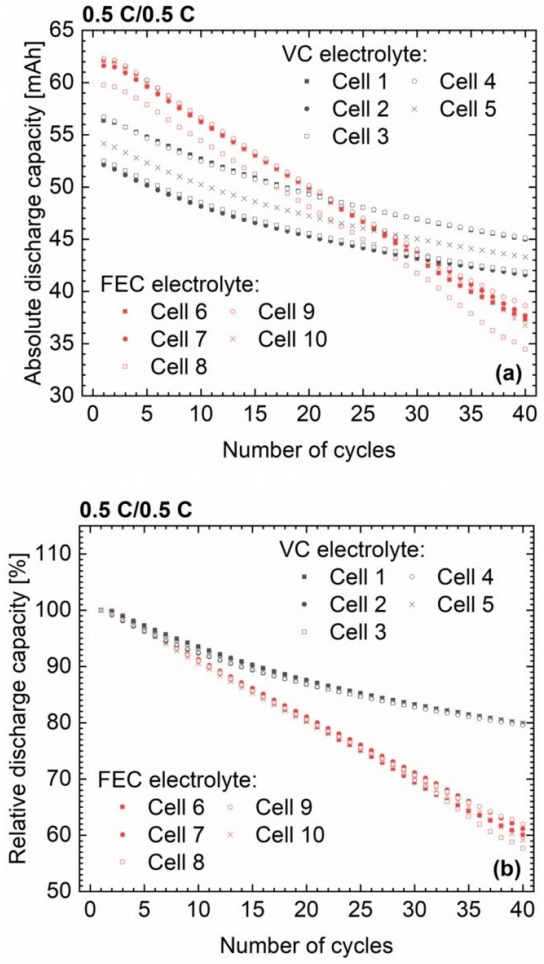

Figure 1. Absolute discharge capacities (a) and relative discharge capacities (b) from NCM622/silicon-graphite pouch cells cycled at 0.5 C/0.5 C in dependence on the number of cycles. The red and black symbols indicate the values from the cells with the FEC electrolyte and the cells with the VC electrolyte, respectively.

silicon particles during the first cycle of the formation should be responsible for a strong loss of cycleable lithium and the resulting low coulombic efficiencies of the first cycle. As a result, the amount of cycleable lithium in the cell is already significantly reduced after formation, which is why the initial discharge capacities in Figure 1a are distinctly lower than the theoretical discharge capacity of the cells. Interestingly, the absolute discharge capacities of the cells with the FEC electrolyte are lower than those of the cells with the VC electrolyte from the 30th cycle (see Figure 1a). As can be concluded from Figure 1b, the capacity retention from the cells with the FEC electrolyte is worse than those from the cells with the VC electrolyte. The relative discharge capacities of the cells with the FEC and VC electrolyte reach 80 % already after about 20 and 40 cycles, respectively (see Figure 1b). The $LiCoO_2$ (LCO)/silicon-alloy-graphite pouch cells investigated by Petibon et al. reached a relative discharge capacity of 80 % only after about 250 cycles,[21] which indicates better cyclability. However, it must be taken into account that Petibon et al. did not use silicon as anode active material in their pouch cells like in this study, but a silicon-alloy.[21] The use of silicon-alloy instead of silicon enables higher capacity retention,[21] which could explain the better cyclability of the LCO/silicon-alloy-graphite pouch cells from Petibon et al. compared to our NCM622/silicon-graphite pouch cells. However, the silicon-alloy used by Petibon et al. has a significantly lower specific capacity (1180 mAh g^{-1})[21] compared to pure silicon (about 3600 mAh g^{-1}).[1–3] As a higher specific capacity of the anode active material leads to a higher energy density of the battery cell, it is desirable to also investigate the capacity loss mechanisms of cells with anodes that contain silicon particles instead of silicon-alloy particles. In fact, the limited cyclability of our self-made NCM622/silicon-graphite pouch cells can be ascribed to the silicon particles (or more precisely the massive SEI growth on the silicon particles), since equivalent self-made NCM622/graphite pouch cells from our previous study without silicon reached a relative discharge capacity of 80 % only after 700–1100 cycles.[23]

Investigation of the Electrolyte Decomposition

Figure 2a indicates the average decomposed amounts of substance or consumptions of the electrolyte components in the cells with the VC electrolyte after formation and after the 40 cycles. Figure 2b shows the equivalent average consumptions of the electrolyte components in the cells with the FEC electrolyte.

The consumptions shown in Figure 2a suggest that VC is almost exclusively consumed in the cells with the VC electrolyte during formation and following cycling, which is consistent with the reported preferential reduction of VC on graphite anodes in lithium-ion battery cells.[27–30] The reduction potential of VC is higher than those of DMC, which leads to a preferential reduction of VC at the anode.[31] As a result, VC can inhibit the DMC reduction,[30] which is in agreement with the low DMC consumptions and the high VC consumptions (see Figure 2a). However, VC cannot prevent completely the DMC decomposition, as can be observed in Figure 2a. This observation is surprising, as the initial electrolyte 1 M $LiPF_6$ in VC:DMC from these cells has a very high VC concentration that should be high enough for a complete suppression of the electrochemical DMC decomposition. No significant $LiPF_6$ decomposition in the cells with the VC electrolyte during formation and following cycling can be found (see Figure 2a).

Figure 2b reveals that FEC is exclusively decomposed in the cells with the FEC electrolyte during formation and subsequent cycling. No significant decomposition of DMC, Li^+, and PF_6^- in the cells with the FEC electrolyte during formation and following cycling can be found. The average DMC consumption in the cells with the FEC electrolyte after formation is even slightly negative. This phenomenon can be ascribed to the fact that the electrolyte amount filled into the cell during cell assembly is not always exactly equal. As a result, it is possible that the initial electrolyte mass and thereby the initial DMC amount are by chance slightly lower in some cells compared to other cells. If the initial electrolyte masses in the three fresh

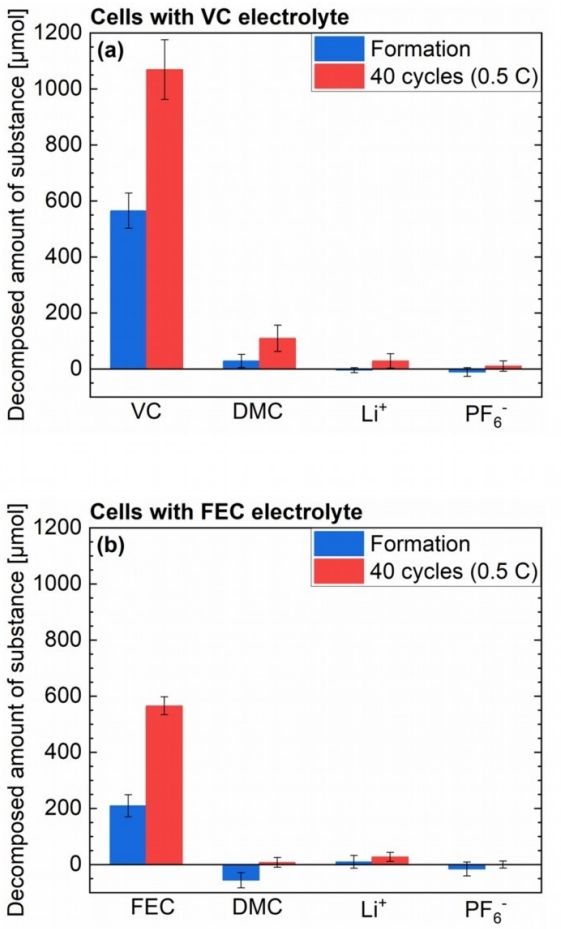

Figure 2. Average consumptions of the electrolyte components in the NCM622/silicon-graphite pouch cells with the VC electrolyte (a) and in the NCM622/silicon-graphite pouch cells with the FEC electrolyte (b) after formation and after the 40 cycles at 0.5 C/0.5 C. The calculations of the average consumptions of the electrolyte components and the associated errors are specified in section SI-4 of the supplementary information. The analyzed electrolytes are extracted from three equally treated cells with the FEC electrolyte and three equally treated cells with the VC electrolyte, so that three independent single values are determined in each case, from which the indicated average consumptions are calculated.

cells are slightly lower than the initial electrolyte masses in the three cells after formation, and if DMC is also electrochemically stable during formation, slightly negative DMC consumptions after formation might be obtained. The exclusive FEC decomposition in the cells with the FEC electrolyte (see Figure 2b) is consistent with the reported exclusive FEC decomposition in lithium-ion battery cells with silicon-containing electrodes.[8] It is known from literature that the reduction potential of FEC is higher than the reduction potential of DMC, which leads to a preferential reduction of FEC.[31]

Interestingly, the VC consumptions in the cells with the VC electrolyte are considerably higher than the FEC consumptions in the cells with the FEC electrolyte during formation and subsequent cycling, as can be observed in Figure 2. However, the absolute discharge capacities after 40 cycles from the cells with the VC electrolyte are even higher than those from the cells with the FEC electrolyte, as can be seen in Figure 1a. Consequently, the irreversible capacity losses and thus also the electrolyte reduction should be rather stronger in the cells with the FEC electrolyte than in the cells with the VC electrolyte during formation and the subsequent 40 cycles. The relatively high VC consumptions (see Figure 2a) and the relatively low FEC consumptions (see Figure 2b) contradict this expectation. The high number of consumed cycleable lithium-ions per reductively decomposed FEC molecule and the low number of consumed cycleable lithium-ions per reductively decomposed VC molecule (see below) are the cause of this apparent contradiction. As a result, a relatively low FEC consumption can be accompanied by a relatively high irreversible capacity loss, whereas a relatively high VC consumption can be associated with a relatively low irreversible capacity loss.

Investigation of the Gas Evolution

The average amounts of the gases released in the pouch cells, namely hydrogen (H_2), methane (CH_4), carbon monoxide (CO), ethylene (C_2H_4), ethane (C_2H_6), and carbon dioxide (CO_2) can be seen in Figure 3a and Figure 3b, respectively.

The gas amounts in the cells with the VC electrolyte and the FEC electrolyte are by orders of magnitude lower than the VC and FEC consumptions (see Figure 2a and Figure 2b), which suggests that none of the end products from the VC and FEC reduction is gaseous. Slight amounts of CH_4 are detected after formation and subsequent cycling (see Figure 3a and Figure 3b). According to literature, the reduction of one DMC molecule yields one CH_4 molecule.[30] Accordingly, the slight amounts of CH_4 in the cells after formation and following cycling (<15 µmol) indicate the reduction of only slight DMC amounts (<15 µmol). In case of the cells with the FEC electrolyte, the slight DMC decomposition is not detected directly in the electrolyte (see Figure 2b) because the determination of the consumption of the electrolyte components is not sensitive enough to detect the decomposition of such slight DMC amounts. Since the average consumption of VC and FEC after 40 cycles (about 1070 µmol and 570 µmol, respectively) is orders of magnitude higher than <15 µmol (see Figure 2a and Figure 2b), the detected CH_4 does not contradict the observed almost exclusive decomposition of VC and FEC in the cells with the VC and FEC electrolyte, respectively.

According to literature, the main gas product from the VC reduction during formation and following cycling is CO_2.[30,32,33] However, the average amount of CO_2 evolved during formation (see Figure 3a) is by orders of magnitude lower than the average VC consumption during formation in the cells with the VC electrolyte (see Figure 2a). Moreover, no further CO_2 is evolved in the cells with the VC electrolyte after formation during the following 40 cycles (see Figure 3a) despite a simultaneous ongoing VC consumption (see Figure 2a). Consequently, the CO_2 evolution can be attributed to a minor side reaction of the reductive decomposition of VC, as described in literature.[32] The major decomposition pathway of VC does not include the formation of CO_2.[32]

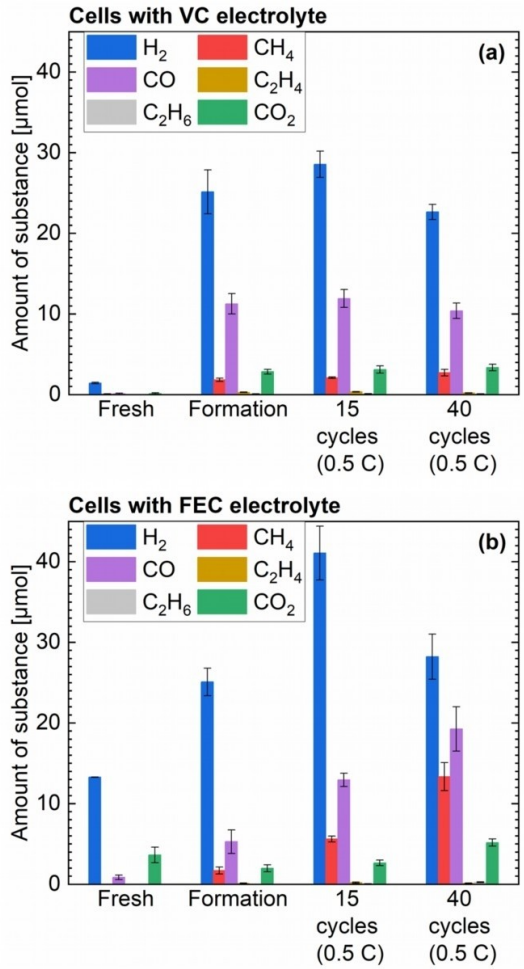

Figure 3. Average amounts of the detected gases in the NCM622/silicon-graphite pouch cells with the VC electrolyte (a) and in the NCM622/silicon-graphite pouch cells with the FEC electrolyte (b). The analyzed gases are extracted from cells before formation, after formation, after the 15 cycles at 0.5 C/0.5 C, and after the 40 cycles at 0.5 C/0.5 C. The calculation of these average gas amounts and the associated errors is described in section SI-3 of the supplementary information. For each of the aging stages, the investigated gases are extracted from two individual, but equally treated cells to obtain two single values, which are then averaged.

Interestingly, no considerable increase of the average CO_2 amount during formation and following cycling can be observed in case of the cells with the FEC electrolyte (see Figure 3b). From literature it is known that the reductive decomposition of FEC at the anodes yield CO_2.[8,34] Jung et al. found that one CO_2 molecule is released for every reduced FEC molecule in lithium-ion battery cells with silicon-containing anodes.[8] According to this, the consumption of the about 570 µmol FEC during formation plus the subsequent 40 cycles (see Figure 2b) should be accompanied by a simultaneous formation of 570 µmol CO_2 in the cells with the FEC electrolyte. However, the average CO_2 amount in the cells with the FEC electrolyte after the 40 cycles is by orders of magnitude lower than these 570 µmol, as can be seen in Figure 3b. This discrepancy could be attributed to a CO_2 consumption subsequent to the CO_2 formation in the cells with the FEC electrolyte during formation and following cycling. In this context, it is important to note that Jung et al. found the release of one CO_2 molecule per decomposed FEC molecule by means of on-line electrochemical mass spectrometry (OEMS) measurements.[8] The used OEMS cell had a huge volume of 9.5 ml and thus also a large gas head space, while the silicon-containing electrode in the OEMS cell had a diameter of only 15 mm.[8] As a result, the evolved CO_2 could rapidly diffuse away from the silicon-containing electrode into the large gas head space, so that the accumulated CO_2 in the gas head space could possibly not be decomposed at the electrode. In contrast, the pouch cells examined in the present work have no gas head space, so that the released CO_2 cannot rapidly diffuse away from the anodes into a separated gas head space. Consequently, the formed CO_2 might be reduced after its evolution instead of accumulating in the cell. In fact, a reductive decomposition of CO_2 in lithium-ion battery cells during formation and following cycling is described yielding SEI components, such as Li_2CO_3.[13,35,36] Thus, it can be assumed that the reductive FEC decomposition is initially associated with the evolution of CO_2, but CO_2 is mainly further decomposed to additional SEI material.

Investigation of the Electrode Surfaces

XPS is applied for the examination of anodes to identify solid products from the reductive decomposition of VC and FEC. The C1s and O1s photoelectron spectra of the anodes from the cells with the VC electrolyte can be seen in Figure 4a and Figure 4c, respectively. The C1s and O1s photoelectron spectra of the anodes from the cells with the FEC electrolyte are displayed in Figure 4b and Figure 4d, respectively.

As can be observed in Figure 4a, the graphite peak (red) is strongly pronounced in the C1s spectrum of the anode from the fresh cell with the VC electrolyte. Notably, the graphite peak is absent in the C1s spectrum of the anode from the cell with the VC electrolyte after formation (see Figure 4a). Besides, the silicon peak (Si^0 2p3 peak at around 99.5 eV), as well as the silicon oxide peak (SiO_2 2p3 peak at around 103.7 eV) are also absent in the Si2p spectrum of the anode from the cell with the VC electrolyte after formation, as can be concluded from Table T-S5 in the supplementary information. The absence of the graphite peak, the silicon peak, and the silicon oxide peak in the spectra after formation suggests that the thickness of the SEI on the graphite particles and the silicon particles is greater than 5–10 nm (information depth of XPS) already after formation in the cells with the VC electrolyte. The silicon oxide peak in the Si2p spectra of the anodes from fresh cells can be attributed to the presence of surface layers of silicon oxide on the silicon particles, which are formed by the reaction of the silicon with the oxygen from the ambient air during storage of the anodes before cell assembly. In the C1s spectrum of the anode from the cell with the VC electrolyte after formation (see Figure 4a), the C_a peak (287.7 eV, light green) and the C_b peak (291.3 eV, purple) are strongly pronounced. In the O1s spectrum of the anode from the cell with the VC electrolyte after formation (see Figure 4c), the O_a peak (532.9 eV, pink) and the O_b peak (534.5 eV, purple) are dominant. According to literature,

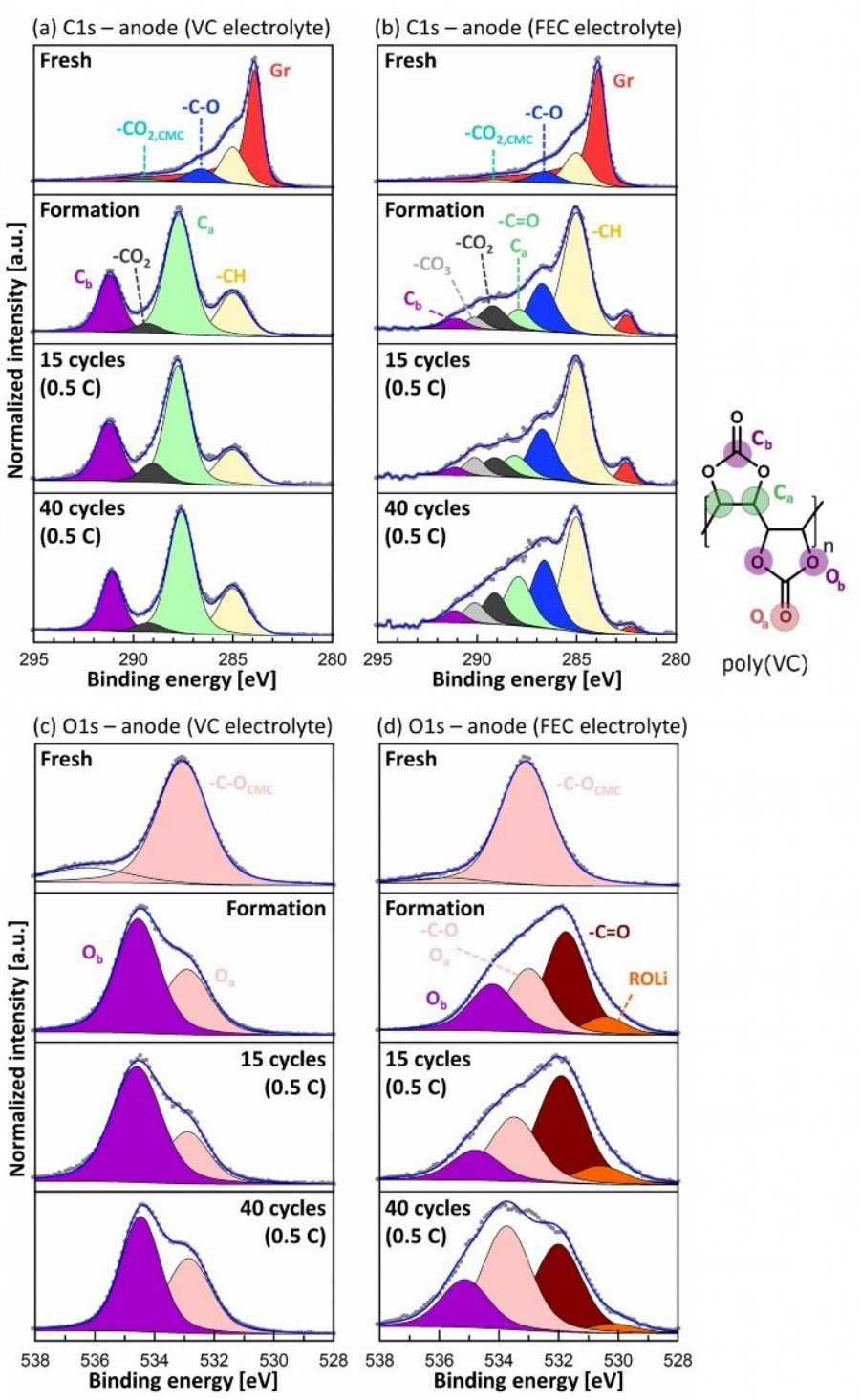

Figure 4. C1s spectra (a) and O1s spectra (c) of anodes from a fresh cell, a cell after formation, a cell after 15 cycles at 0.5 C/0.5 C, and a cell after 40 cycles at 0.5 C/0.5 C each with the VC electrolyte. Furthermore, C1s spectra (b) and O1s spectra (d) of anodes from a fresh cell, a cell after formation, a cell after 15 cycles at 0.5 C/0.5 C, and a cell after 40 cycles at 0.5 C/0.5 C each with the FEC electrolyte are depicted.

the C_a peak, the C_b peak, the O_a peak, and the O_b peak can be ascribed to poly(VC) (structural formula see Figure 4), which represents a VC decomposition product.[28] The C1s and O1s spectra of the anodes after the 15 cycles and the 40 cycles are similar to the C1s and O1s spectrum of the anode after formation, as can be seen in Figure 4a and Figure 4c. Furthermore, the compounds characteristic for poly(VC), namely C_a, C_b, O_a, and O_b, are abundant in the SEI from the cells with the VC electrolyte after formation and after following cycling, as can be concluded from the atomic percentages of the compounds

determined by XPS (see Table T-S5 in the supplementary information). These findings indicate that poly(VC) is the main component of the SEI from the cells with the VC electrolyte, which is in agreement with the pronounced VC decomposition (see Figure 2a). Moreover, the atomic percentages of lithium in the surface layers of the anodes from the cells with the VC electrolyte are low or even negligible (see values from Li1s spectra in Table T-S5 in the supplementary information), which indicates a low lithium content of the SEI from the cells with the VC electrolyte.

The graphite peak is also dominant in the C1s spectrum of the anode from the fresh cell with the FEC electrolyte (see Figure 4b). The height of the graphite peak decreases continuously during formation and the following 40 cycles, as can be seen in Figure 4b. This height reduction of the graphite peak can be attributed to the continuous growth of the SEI during formation and following cycling. However, the graphite peak is still visible even in the C1s spectrum of the anode from the cell with the FEC electrolyte after the 40 cycles. From this it can be concluded that the thickness of the SEI on the graphite particles is always less than 5–10 nm (information depth of XPS) during formation and the following 40 cycles in the cells with the FEC electrolyte. The binding energy of the graphite peak is shifted towards lower binding energies after formation and subsequent cycling, as can be seen in Figure 4b. Although the examined anodes were extracted in the delithiated state from completely discharged cells, this shift could indicate some trapped lithium in the graphite. However, an electric potential gradient at the buried interface between SEI and graphite is likely responsible for this graphite peak shift, as reported in literature.[37] The silicon peak (Si^0 2p3 peak at around 99.5 eV) and the silicon oxide peak (SiO_2 2p3 peak at around 103.7 eV) are admittedly (almost) not present in the Si2p spectrum of the anode from the cell with the FEC electrolyte after formation, as can be concluded from Table T-S6 in the supplementary information. Indeed, the peaks of lithiated silicon (Li_xSi_y peak at around 97.4 eV) and lithiated silicon oxide (Li_xSiO_y peak at around 100.5 eV) are present in the Si2p spectra of the anodes from the cells with the FEC electrolyte after formation and after the 15 cycles (see Table T-S6 in the supplementary information). However, lithiated silicon and lithiated silicon oxide are no longer detectable on the anode after the 40 cycles, as can be seen in Table T-S6 in the supplementary information. Consequently, the thickness of the SEI on the silicon particles in the cells with the FEC electrolyte seems to be greater than 5–10 nm (information depth of XPS) only after the 40 cycles. Since all anodes are extracted in the delithiated state from discharged cells, the detected lithiated silicon might be ascribed to lithium trapping in the silicon. This phenomenon might be explained by an accumulation of electrochemically inactive Li_xSi_y in the surface layer of the silicon particles during formation and following cycling, as described in literature.[38] The detected lithiated silicon oxide or lithium silicate might be attributed to lithium trapping in the silicon oxide layers of the silicon particles. Correspondingly, lithium silicate remains electrochemically inactive once it is formed according to literature.[39,40] As can be seen in Figure 4b and Figure 4d, the peaks characteristic for poly(VC) (C_a peak, C_b peak, O_a peak, and O_b peak) are present, but not dominating in the C1s spectra and the O1s spectra of the anodes from the cells with the FEC electrolyte after formation and after subsequent cycling. This finding together with the observed exclusive decomposition of FEC (see Figure 2b) suggest that poly(VC) is not a main decomposition product from FEC. Thus, only a small fraction of the consumed FEC is electrochemically decomposed to poly(VC). Correspondingly, the decomposition of FEC yields poly(VC) and LiF.[18,41] Furthermore, the -CO_3 peak (290.1 eV, light grey) and the –CO_2 peak (289.1 eV, dark grey) can be identified in the C1s spectra of the anodes from the cells with the FEC electrolyte after formation, after the 15 cycles, and after the 40 cycles (see Figure 4b). The -CO_3 peak can be ascribed to lithium carbonate, while the -CO_2 peak might be related to the presence of lithium oxalate and lithium formate.[42] This deposition of lithium carbonate, lithium oxalate, and lithium formate on the anodes can be attributed to the reduction of CO_2,[35] which is formed by the reductive decomposition of FEC.[8] Additionally, the –C–O peak (286.7 eV, blue) is strongly pronounced in the C1s spectra of the anodes from the cells with the FEC electrolyte after formation, after the 15 cycles, and after the 40 cycles (see Figure 4b). From literature it is known that the –C–O peak is the dominant peak in the C1s spectrum from polyethylene oxide (PEO).[43] According to this, a deposition of PEO or a PEO-type polymer on the anodes during formation and following cycling in the cells with the FEC electrolyte might be responsible for the distinct –C–O peaks in Figure 4b. In fact, it is known from literature that the FEC reduction yields PEO that forms part of the SEI.[19] As can be concluded from Table T-S6 in the supplementary information, LiF accumulates in the SEI from the cells with the FEC electrolyte during formation and the following 40 cycles. The data in Table T-S6 in the supplementary information indicate that LiF is a main component of the SEI from the cells with the FEC electrolyte. This finding, as well as the exclusive decomposition of FEC in the cells with the FEC electrolyte (see Figure 2b) indicate that LiF represents a main decomposition product from FEC. Many reports confirm that the FEC reduction in lithium-ion battery cells yields the SEI component LiF among others.[8,16,20,44–46] As can be concluded from the data of the Li1s spectra in Table T-S6 in the supplementary information, the lithium content of the SEI from the cells with the FEC electrolyte is high.

According to the XPS analyses, the thickness of the SEI from the cells with the VC electrolyte is always greater than 5–10 nm, whereas the thickness of the SEI from the cells with the FEC electrolyte is mostly less than 5–10 nm. The thick SEI from the cells with the VC electrolyte and the thin SEI from the cells with the FEC electrolyte can be attributed to the high VC consumptions and the low FEC consumptions (see Figure 2). Consequently, more SEI material is deposited in the cells with the VC electrolyte than in the cells with the FEC electrolyte, so that the thickness of the VC-derived SEI is greater than the thickness of the FEC-derived SEI. The data from the Li1s spectra in the Tables T-S5 and T-S6 in the supplementary information suggest that the lithium content of the SEI from the cells with the VC electrolyte is substantially lower than the lithium

content of the SEI from the cells with the FEC electrolyte. The low number of consumed lithium-ions per reduced VC molecule and the high number of consumed lithium-ions per reduced FEC molecule (see below) are the reasons for the low lithium content of the VC-derived SEI and the high lithium content of the FEC-derived SEI.

Identification of the Cause of Capacity Loss

A lithium-ion battery cell can lose cycleable lithium and thus capacity by SEI formation, irreversible lithium plating, active material loss, and lithium trapping in the active material.[47] Both active material loss and lithium trapping in the active material correspond to a loss of active material that was initially electronically connected to the current collector. In addition, there are parasitic reactions that consume only charge, but not cycleable lithium, such as transfer of transition metals from the cathode to the anode or redox shuttle mechanisms.[47] These parasitic reactions are not associated with a capacity loss of the lithium-ion battery cell.

ICP-OES is applied for the analyses of anodes and cathodes to determine the lithium (Li) amount in the anodes and the Li loss of the cathodes after formation, after the 15 cycles, and after the 40 cycles. Thereby, information about the cause of the capacity loss of the pouch cells can be gained. Each examined cell is in the completely discharged state, meaning all mobile Li is extracted from the anodes. Furthermore, the electron consumption at the anodes is determined based on the cumulative irreversible capacity and the Faraday constant, as described in section SI-7 of the supplementary information. The graphs in Figure 5 display the average Li amounts in the anodes, the average Li losses of the cathodes, and the associated electron consumptions at the anodes. As can be seen in Figure 5, the quantified Li losses of the cathodes are not significantly different from the electron consumptions at the anodes. Thus, the electron consumption at the anodes is (almost) exclusively triggered by a loss of cycleable Li, which is initially present in the cathodes. Consequently, parasitic reactions, which consume electrons, but not cycleable Li at the anodes, barely contribute to the electron consumption at the anodes in the cells with the VC electrolyte and the FEC electrolyte. Furthermore, the Li amounts in the anodes also correspond to the electron consumptions at the anodes, as can be seen in Figure 5. Consequently, the consumption of one electron at the anodes is associated with the trapping of one cycleable Li-ion in the anodes. The slight Li amounts in the fresh anodes (see Figure 5) can be attributed to $LiPF_6$, which is not removed from the anodes during sample preparation. In addition, the Li amounts in the anodes from the cells with the VC electrolyte after the 40 cycles are close to the Li amounts in the anodes from the cells with the FEC electrolyte after the 40 cycles (see Figure 5a and Figure 5b). The Li losses of the cathodes after the 40 cycles are around 2200 µmol (see Figure 5a and Figure 5b), which corresponds to 42 % of the initially present Li in the cathodes (around 5300 µmol).

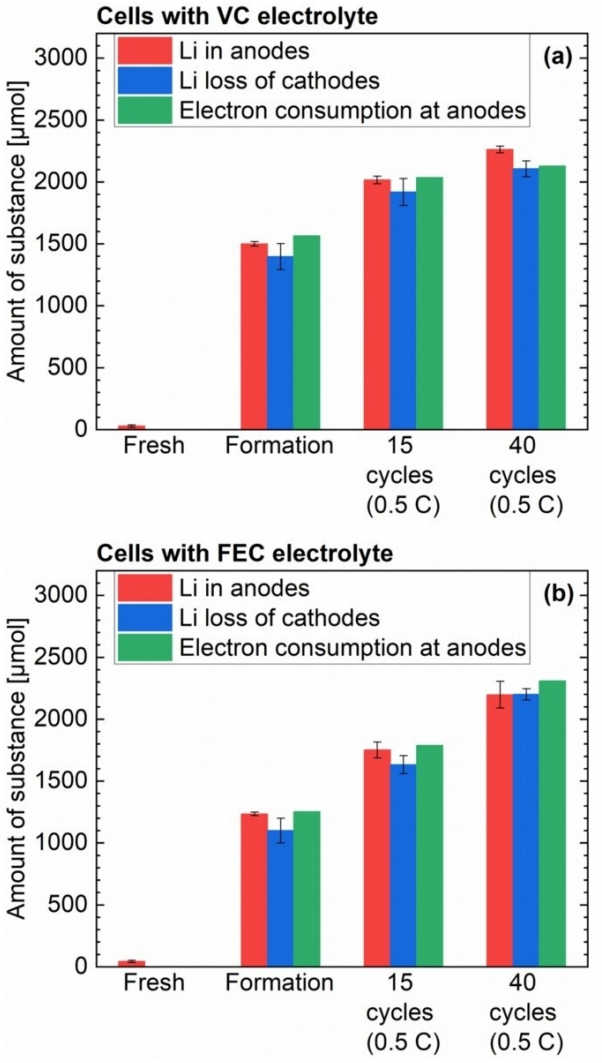

Figure 5. Average amounts of Li in the anodes from the NCM622/silicon-graphite pouch cells with the VC electrolyte (a) and FEC electrolyte (b) before formation, after formation, after 15 cycles at 0.5 C/0.5 C, and after 40 cycles at 0.5 C/0.5 C. Additionally, the average Li losses of the cathodes from these cells can be seen. Besides, the respective electron consumptions at the anodes are shown. For each of these aging stages, the analyzed electrodes are extracted from one cell with the VC electrolyte and one cell with the FEC electrolyte.

The irreversible Li plating should not contribute significantly to the capacity losses of the investigated pouch cells, as the cells are cycled slowly ($\leq$0.5 C) and the theoretical areal capacity of the anodes is distinctly higher than the theoretical areal capacity of the cathodes. To check whether SEI formation or loss of electronically connected active material is responsible for the capacity losses, the areal capacities of electrodes are determined. For that purpose, pouch cells after formation and after 40 cycles at 0.5 C/0.5 C are disassembled in an argon-filled glovebox. Following this, coin cell electrodes are punched out of the anodes and cathodes from these pouch cells. Afterwards, coin cells are assembled with the punched electrodes from the pouch cells (as working electrodes) and Li metal (as counter electrodes). In case of the coin cells with the silicon-graphite electrodes, the charge capacity from the second cycle (at 0.1 C/

0.1 C) is divided by the area of the silicon-graphite electrode resulting in the measured areal capacity. In case of the coin cells with the NCM622 electrodes, the discharge capacity from the second cycle (at 0.1 C/0.1 C) is divided by the area of the NCM622 electrode resulting in the measured areal capacity. The average measured areal capacities of the coin cells with the electrodes from the pouch cells with the VC electrolyte and the FEC electrolyte after formation and after the 40 cycles at 0.5 C/0.5 C are shown in Figure 6a and Figure 6b, respectively. For each examined pouch cell electrode, three coin cells are assembled and cycled resulting in three single values of the areal capacity. Based on respective three single values, the indicated average areal capacities are calculated. The indicated errors of the average areal capacities correspond to the standard deviations of the mean that are calculated by the respective three single values.

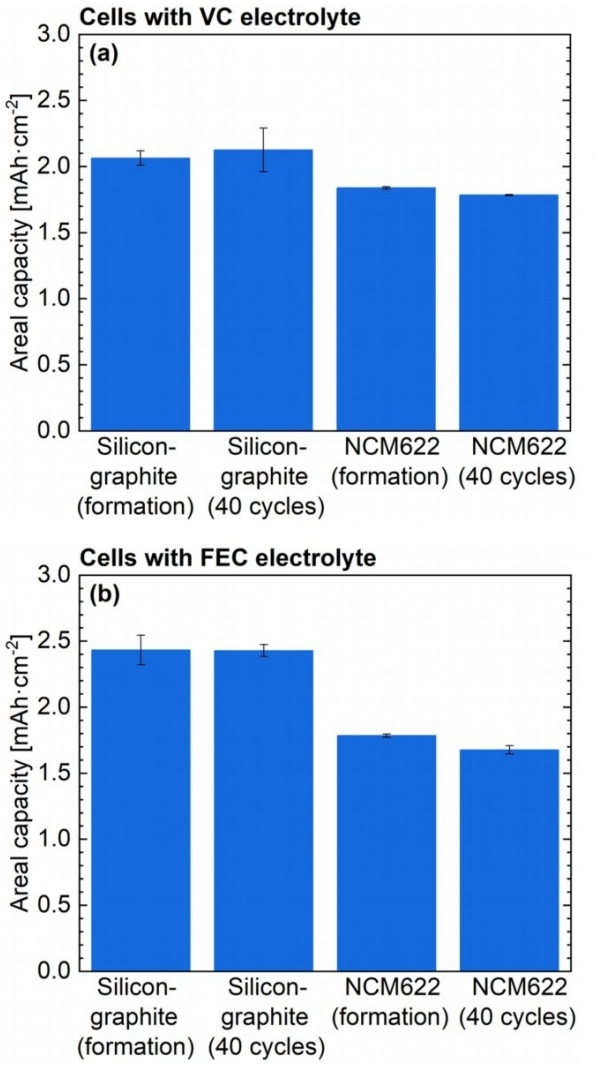

Figure 6. Average areal capacities of the half-cells with the silicon-graphite electrodes and the NCM622 electrodes that are punched out of the anodes and cathodes from the NCM622/silicon-graphite pouch cells with the VC electrolyte (a) and FEC electrolyte (b) after formation and after 40 cycles at 0.5 C/0.5 C.

As can be concluded from Figure 6a and Figure 6b, the areal capacities of the silicon-graphite anodes from the pouch cells with the VC electrolyte and the pouch cells with the FEC electrolyte do not decrease after formation during the following 40 cycles. This observation suggests that a loss of electronically connected anode active material does not contribute to the capacity losses of the NCM622/silicon-graphite pouch cells after formation during the subsequent 40 cycles. Note that the differential capacities plotted against the voltage can be seen in Figure F-S1 in the supplementary information for the half-cells with the silicon-graphite electrodes.

The areal capacities of the NCM622 cathodes from the pouch cells with the VC electrolyte and the FEC electrolyte decrease slightly (about 5 %) after formation during the following 40 cycles (see Figure 6a and Figure 6b). This observation can be attributed to a slight loss of electronically connected cathode active material in the NCM622/silicon-graphite pouch cells during the 40 cycles, because the NCM622 particles lose electrical contact to the current collector owing to crack formation in the NCM622 particles during de-/lithiation. However, around 42 % of the initially present Li from the cathodes are no longer present in the cathodes from the examined pouch cells after the 40 cycles, as already mentioned. Consequently, 42 % of the initially available spaces for Li-ions in the cathodes remain unoccupied after the 40 cycles, so that the slight loss of about 5 % of the spaces for Li-ions in the cathodes should not lead to a capacity loss of the pouch cells. This finding indicates that a loss of electronically connected cathode active material does not contribute to the capacity losses of the NCM622/silicon-graphite pouch cells after formation during the subsequent 40 cycles. Thus, neither an effective loss of electronically connected cathode active material, nor a loss of electronically connected anode active material can be observed after formation during the following 40 cycles. Consequently, the losses of cycleable Li and the consequent capacity losses of the NCM622/silicon-graphite pouch cells after formation during the following 40 cycles are (almost) exclusively caused by trapping of cycleable Li in the SEI.

The measured areal capacities of the NCM622 cathodes after formation (see Figure 6a and Figure 6b) correspond to the theoretically calculated areal capacity of the NCM622 cathodes (1.8 mAh cm^{-2}). Hence, no electronically connected cathode active material is lost during formation in the NCM622/silicon-graphite pouch cells. In contrast, the measured areal capacities of the silicon-graphite anodes after formation (see Figure 6a and Figure 6b) are with about 2.0 mAh cm^{-2}–2.4 mAh cm^{-2} distinctly lower than the theoretically calculated areal capacity of the silicon-graphite anodes (3.0 mAh cm^{-2}). This discrepancy might be partly ascribed to the fact that the specific capacity of silicon (3579 mAh g^{-1}) assumed for the calculation of the theoretical areal capacity of the silicon-graphite anodes is too high. This assumed specific capacity of silicon is the specific capacity of highly lithiated $Li_{15}Si_4$.[1,3] However, the XPS measurements reveal the presence of a surface layer of silicon oxide on the silicon particles from the electrochemically untreated fresh anodes, as already explained. The specific capacity of silicon oxide is only 1708 mAh g^{-1}.[39] Hence, the initially present silicon

oxide layers on the silicon particles from the anodes might be (partly) responsible for the deviation between the measured areal capacities and the theoretically calculated areal capacity of the silicon-graphite anodes. The lithiation of silicon oxide during the first charge partly yields lithium silicate (Li_xSiO_y), which remains electrochemically inactive once it is formed.[39,40] In fact, lithium silicate is detected by XPS in the surface layers of the anodes from the pouch cells with the FEC electrolyte after formation and after the 15 cycles, as already mentioned. Furthermore, an incomplete delithiation of Li_xSi_y during delithiation of the silicon-graphite anodes might also be (partly) responsible for the mentioned deviation between the measured areal capacities and the theoretically calculated areal capacity of the silicon-graphite anodes. In fact, Li_xSi_y is also detected by XPS in the surface layers of the anodes from the pouch cells with the FEC electrolyte after formation and after the 15 cycles, as already described. Hence, part of the silicon oxide and silicon might be irreversibly lithiated during the first charge of the formation in the investigated pouch cells, so that a layer of electrochemically inactive Li_xSiO_y and Li_xSi_y is formed under the SEI on the silicon particles. The resulting trapping of cycleable Li in irreversibly lithiated silicon oxide and silicon corresponds to a loss of electronically connected anode active material. Li_xSiO_y and Li_xSi_y are supposedly not detected in the surface layers of all anodes after formation and after following cycling, as the overlying SEI is often thicker than the information depth of XPS. Thus, the losses of cycleable Li and the consequent capacity losses of the NCM622/silicon-graphite pouch cells during formation (or the first cycle of the formation) can be (almost) exclusively ascribed to trapping of cycleable Li in the SEI and to trapping of cycleable Li in irreversibly lithiated silicon (Li_xSi_y) and silicon oxide (Li_xSiO_y) under the SEI.

Proposed Reactions of the Reductive Decomposition of VC and FEC

An almost exclusive decomposition of VC and FEC during formation and subsequent cycling is found in case of the pouch cells with the VC electrolyte and the FEC electrolyte, respectively. The electrochemical decomposition of VC and FEC can be ascribed to reductive decomposition at the anode or oxidative decomposition at the cathode. For an oxidative decomposition of VC and FEC, the cathode potential must be higher than the oxidation potential of VC and FEC, respectively. According to literature, the oxidation potential of VC is 4.3–4.5 V vs. Li/Li^+,[48,49] while the oxidation potential of FEC is 7.24 V vs. Li/Li^+.[50] This means that even VC is only oxidatively decomposed at cell voltages above 4.3–4.4 V in full-cells with a graphite anode.[49] Correspondingly, Petibon et al. observed that VC was hardly decomposed at the cathode by oxidation, but primarily at the anode by reduction in NCM111/graphite pouch cells, although the cell voltage was held at 4.2 V for 200 hours.[51] Consequently, oxidative decomposition of VC and FEC should not contribute substantially to the observed consumptions of VC and FEC in our NCM622/silicon-graphite pouch cells, whose cell voltage never exceeds 4.2 V during formation and subsequent cycling. Hence, the consumption of VC and FEC in our cells should be induced by their reductive decomposition at the anode. This conclusion is further confirmed by the mass increase of the anodes during formation and the following 40 cycles and the simultaneous mass loss of the cathodes (see section SI-8 and Figure F-S2 in the supplementary information). These mass increases of the anodes correspond to the sum of the average lithium mass in the anodes after the 40 cycles plus the average mass of the consumed VC (in case of the cells with the VC electrolyte) or FEC (in case of the cells with the FEC electrolyte) after the 40 cycles. Simultaneously, the mass losses of the cathodes after the 40 cycles correspond to the average mass of the lost lithium from the cathodes after the 40 cycles. These observations confirm that VC and FEC is (almost) exclusively decomposed by reduction at the anode together with lithium to solid SEI material. If a substantial amount of VC and FEC would be oxidatively decomposed to solid products on the cathode surface, the cathodes would not lose, but gain mass during formation and subsequent cycling. In fact, VC can be oxidatively decomposed at high cathode potentials to poly(VC) that is deposited on the cathode.[48] But in light of our experimental results, it is reasonable to assume that VC and FEC is exclusively decomposed by reduction at the anode in the cells with the VC and FEC electrolyte, respectively. To understand the mechanisms for the reductive decomposition of VC and FEC, it is helpful to examine the correlation between the charge consumption (or electron consumption) at the anodes and the VC and FEC consumption, respectively. The charge consumption at the anodes corresponds to the cumulative irreversible capacity that is calculated according to Equation 9 of the supplementary information. The y-axis of Figure 7a displays the average cumulative irreversible capacities of the NCM622/silicon-graphite pouch cells with the VC electrolyte, whose electrolytes are analyzed after formation, after the 15 cycles, and after the 40 cycles. The x-axis of Figure 7a indicates the average amounts of consumed VC (VC consumptions) for these cells. The y-axis of Figure 7b indicates the average cumulative irreversible capacities of the NCM622/silicon-graphite pouch cells with the FEC electrolyte, whose electrolytes are analyzed after formation, after the 15 cycles, and after the 40 cycles. The average amounts of consumed FEC (FEC consumptions) in these cells are indicated by the x-axis of Figure 7b. The average cumulative irreversible capacities and average consumptions shown in Figure 7a and Figure 7b are the means of three single values, since the electrolytes from three equally treated cells are analyzed in each case. The associated errors are the standard deviations of the mean that are calculated based on the respective three single values.

The electron consumption at the anodes corresponds to the cumulative irreversible capacity (in As) divided by the Faraday constant. The number of consumed electrons per consumed VC molecule (the e^-/VC value) is the quotient of the electron consumption at the anodes and the VC consumption. The number of consumed electrons per consumed FEC molecule (the e^-/FEC value) corresponds to the quotient of the electron consumption at the anodes and the FEC consumption. The e^-/VC value and the e^-/FEC value reveal how many electrons are

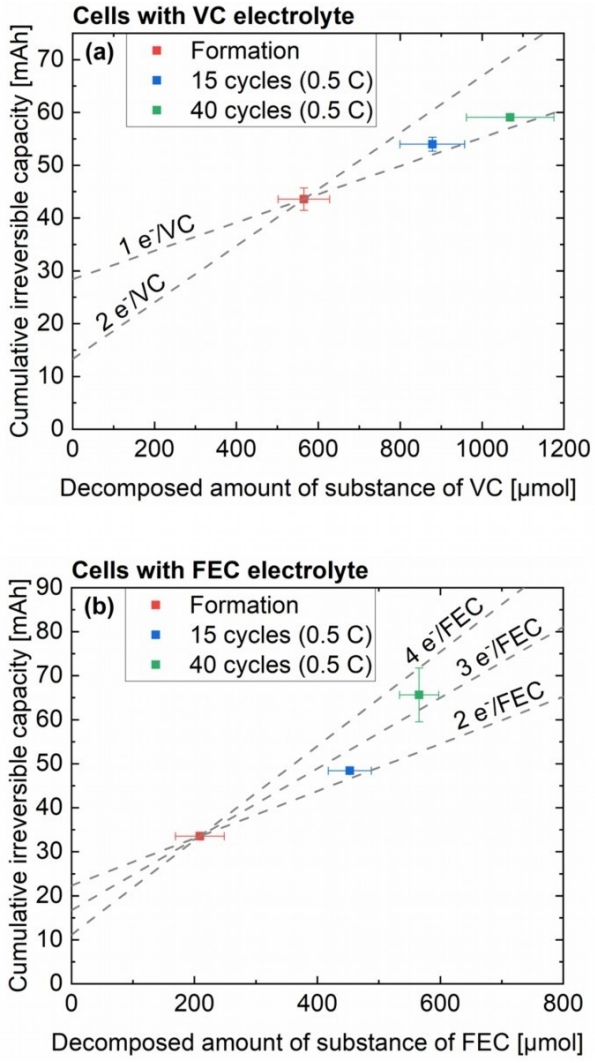

Figure 7. (a) Average cumulative irreversible capacities of the NCM622/silicon-graphite pouch cells with the VC electrolyte plotted against the average VC consumptions in these cells. (b) Average cumulative irreversible capacities of the NCM622/silicon-graphite pouch cells with the FEC electrolyte plotted against the average FEC consumptions in these cells. Both diagrams show the values for the cells, whose electrolytes are analyzed after formation (red squares), after the 15 cycles at 0.5 C/0.5 C (blue squares), and after the 40 cycles at 0.5 C/0.5 C (green squares).

consumed by the reductive decomposition of one VC molecule and one FEC molecule, respectively. Based on the average cumulative irreversible capacity and the average VC consumption after the 40 cycles shown in Figure 7a (about 59 mAh and about 1070 µmol, respectively), an e^-/VC value of 2.1 ± 0.3 is calculated. Hence, it could be concluded that the reductive decomposition of one VC molecule is associated with the consumption of two electrons. Based on the average cumulative irreversible capacity and the average FEC consumption after the 40 cycles indicated in Figure 7b (about 66 mAh and about 570 µmol, respectively), an e^-/FEC value of 4.3 ± 0.3 is calculated. From this, a four electron reduction of FEC could be concluded, which is consistent with the four electron reduction of FEC proposed by Jung et al.[8] Jung et al. determined a similar e^-/FEC value of 3.8 ± 0.6 using a different determination method,[8] which indicates that our method for the determination of the e^-/FEC value or the e^-/VC value leads to valid results. However, it must be taken into account that electrons are additionally consumed at the anodes by the mentioned irreversible lithiation of silicon and silicon oxide during formation, which is not associated with a consumption of VC or FEC. As a result, the reductive decomposition of one VC molecule and one FEC molecule should consume less than two electrons and four electrons, respectively. Irreversible lithium plating should not occur in the investigated pouch cells due to the low charge currents ($\leq$ 0.5 C) and the capacitively oversized anodes. Furthermore, (almost) no loss of electronically connected active material can be observed in the pouch cells after formation during the subsequent 40 cycles, as already mentioned. Hence, irreversible lithium plating and loss of electronically connected active material should not contribute substantially to the electron consumption at the anodes after formation during the following 40 cycles. Additionally, parasitic reactions, which consume electrons, but not cycleable lithium at the anodes, barely contribute to the electron consumption at the anodes in the cells, as already explained. Consequently, it is reasonable to assume that the electron consumption at the anodes after formation during the following 40 cycles is (almost) exclusively induced by SEI growth. Because an (almost) exclusive decomposition of VC and FEC is observed in the cells with the VC electrolyte and the FEC electrolyte, respectively (see Figure 2), it can be assumed that the SEI growth in these cells is (almost) exclusively induced by the reductive decomposition of VC or FEC. Thus, it can be concluded that the electrons are (almost) exclusively consumed by the reductive decomposition of VC or FEC after formation during following cycling. Consequently, it is reasonable to determine how many electrons are consumed for each VC molecule or FEC molecule that is consumed after formation during following cycling by means of the e^-/VC ratio or the e^-/FEC ratio after formation during following cycling. The dashed lines in the plots in Figure 7a and Figure 7b indicate the relevant e^-/VC ratios and e^-/FEC ratios after formation during following cycling. The dashed lines in Figure 7a indicate the correlation between the cumulative irreversible capacity and the VC consumption in case of a one electron reduction (1 e^-/VC line with a corresponding slope of 0.02680 mAh/µmol) and a two electron reduction (2 e^-/VC line with a corresponding slope of 0.05360 mAh/µmol). Accordingly, the dashed lines in Figure 7b indicate the relationship between the cumulative irreversible capacity and the FEC consumption in case of a two electron reduction (2 e^-/FEC line with a corresponding slope of 0.05360 mAh/µmol), a three electron reduction (3 e^-/FEC line with a corresponding slope of 0.08040 mAh/µmol), and a four electron reduction (4 e^-/FEC line with a corresponding slope of 0.1072 mAh/µmol). The dashed lines in Figure 7 go through the data points from the cells after formation because these data points serve as reference points in this context.

The data points from the cells after the 15 cycles and after the 40 cycles lie just slightly above the dashed line that indicates the 1 e^-/VC ratio, as can be seen in Figure 7a. From this it can be concluded that the reductive decomposition of

one VC molecule consumes one electron. Moreover, the electron consumptions at the anodes correspond to the lithium amounts in the anodes from the cells with the VC electrolyte, as can be observed in Figure 5a. Hence, one lithium-ion is deposited on the anode for every electron consumed at the anode in the cells with the VC electrolyte. Consequently, the reductive decomposition of one VC molecule is associated with the consumption of one electron and one lithium-ion at the anode. Furthermore, the main component of the SEI from the cells with the VC electrolyte is poly(VC), as already described. Based on these findings, the reaction of the reductive decomposition of VC can be proposed, which is shown in Figure 8. Accordingly, one lithium-ion and one VC molecule are reduced by uptake of one electron at the anode yielding one monomer of a lithium-containing poly(VC). The repetition of this process yields a lithium-containing poly(VC) that forms the SEI. According to literature, most of the VC molecules directly react to lithium-free poly(VC) due to an attack by the initial VC reduction product.[32,52] Indeed, this reaction of many VC molecules to poly(VC) proposed in literature leads to the consumption of only one electron (meaning $e^-/VC < 1$) and no lithium-ions, which contradicts the observation in this study that the reductive decomposition of one VC molecule consumes one electron and one lithium-ion. Kuai et al., however, proposed the formation of a lithium-containing poly(VC) based on ab initio molecular dynamic (AIMD) simulations.[53] According to this proposal, one lithium-ion is admittedly consumed for each consumed VC molecule in agreement with our observation. However, the formation of one lithium-containing poly(VC) only consumes one electron (meaning $e^-/VC < 1$) according to this proposal from Kuai et al.,[53] which contradicts our observation that the reduction of one VC molecule consumes one electron ($e^-/VC = 1$). Nevertheless, the lithium-containing poly(VC) (see Figure 8) might have a similar structural formula as the lithium-containing poly(VC) proposed by Kuai et al.[53] The trapping of cycleable lithium in the SEI by the proposed VC reduction (see Figure 8) is almost exclusively responsible for the capacity loss of the investigated pouch cells with the VC electrolyte after formation during subsequent cycling. To the best of our knowledge, this is the first empirical evidence that the reductive decomposition of one VC molecule consumes one electron and one lithium-ion in lithium-ion battery cells.

As can be concluded from Figure 7b, the reductive decomposition of one FEC molecule probably consumes three electrons. The data point from the cells after the 15 cycles is between the dashed line that indicates the 2 e^-/FEC ratio and the dashed line that indicates the 3 e^-/FEC ratio. The data point from the cells after the 40 cycles is between the dashed line that indicates the 3 e^-/FEC ratio and the dashed line that indicates the 4 e^-/FEC ratio. For this reason, a three electron reduction of FEC is assumed, which admittedly contradicts the four electron reduction of FEC proposed by Jung et al.[8] One reason for this discrepancy is that Jung et al. delithiated the silicon-containing electrode using CC mode without a constant voltage (CV) step before the electrolyte analyses.[8] As a result, not all mobile lithium-ions and electrons were extracted from the silicon-containing electrode due to the polarization, so that the cumulative irreversible capacity (electron consumption) and thus also the number of consumed electrons per reduced FEC molecule was overestimated. In contrast, herein a four hours long CV step after the final discharge of the cells is applied before the electrolyte analyses, which ensures that all mobile lithium-ions and electrons are extracted from the anodes. As a result, the electron consumption at the anodes is lower, so that the number of consumed electrons per reduced FEC molecule is lower than four. Indeed, Wetjen et al. also used a CV step at the end of the final delithiation of the silicon-graphite anode (with a current limit of 0.02 C) and observed that the number of consumed electrons per reduced FEC molecule is 3.0 ± 0.2.[14] The electron consumptions at the anodes are close to the lithium amounts in the anodes from the cells with the FEC electrolyte, as can be observed in Figure 5b. Consequently, one lithium-ion is deposited on the anode for every electron consumed at the anode in the cells with the FEC electrolyte. Thus, the reductive decomposition of one FEC molecule probably consumes three electrons and three lithium-ions at the anode. Additionally, the SEI from the cells with the FEC electrolyte contains LiF, PEO (or a PEO-type polymer), lithium carbonate, lithium oxalate, and lithium formate, as already described. Leung et al. proposed that the one electron reduction of FEC yields a FEC-radical anion that is decomposed to LiF, CO_2, and a vinoxyl-radical.[34] In fact, Schroder et al. concluded from their experimental results that FEC reduction yields LiF.[54] Shkrob et al. detected experimentally the formation of the vinoxyl-radical by the FEC decomposition.[55] Furthermore, Jung et al. found experimentally that one CO_2 molecule is released for each reductively decomposed FEC molecule.[8] Consequently, it is reasonable to assume that one FEC molecule, one

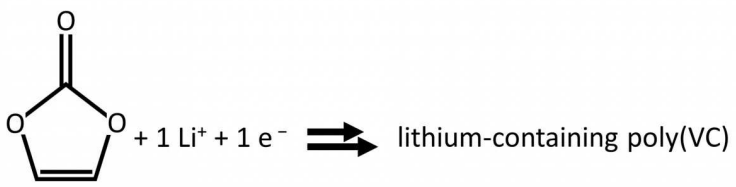

Figure 8. Proposed reaction of the reductive decomposition of VC. One lithium-ion and one VC molecule are reduced by uptake of one electron yielding lithium-containing poly(VC).

lithium-ion, and one electron actually react to one LiF molecule, one CO_2 molecule, and one vinoxyl-radical. However, the CO_2 released by the FEC reduction is further reduced yielding additional SEI material as no substantial CO_2 amounts are detected in the cells with the FEC electrolyte (see Figure 3b). According to this, Krause et al. found that initially present CO_2 is gradually consumed during cycling in lithium-ion battery cells leading to SEI buildup.[36] Schwenke et al. observed that the SEI components lithium oxalate, lithium formate, and especially lithium carbonate are formed by the reductive decomposition of CO_2 in lithium-ion battery cells.[35] Solchenbach et al. found that two electrons are consumed for each reductively decomposed CO_2 molecule.[13] Hence, it is assumed in the following that the reductive decomposition of one CO_2 molecule consumes two electrons. Vinoxyl-radicals can initiate polymerizations that eventually yield a highly cross-linked network.[56] Moreover, it is reported in literature that the FEC-derived SEI is mainly composed of cross-linked PEO.[19] Consequently, it is reasonable to assume that the vinoxyl-radicals accumulate on the anode surface during cycling and mostly react with each other leading to the formation of a cross-linked PEO-type polymer. The following mechanism for the reductive decomposition of FEC is proposed based on the results from this work and the mentioned findings from literature: In the first step, one FEC molecule, one lithium-ion, and one electron react with each other to form one LiF molecule, one CO_2 molecule, and one vinoxyl-radical (consumption of the 1st electron). The released CO_2 molecule, two lithium-ions, two electrons, and possibly other molecules react with each other to form lithium carbonate (Li_2CO_3), lithium oxalate ($Li_2C_2O_4$), or lithium formate (HCO_2Li) (consumption of the 2nd and 3rd electron). Admittedly, precise reactions of the CO_2 reduction cannot be proposed at this point. To the best of our knowledge, plausible chemical equations for a two electron reduction of CO_2 in lithium-ion battery cells are also not described in literature so far. The formed vinoxyl-radicals polymerize with each other without consumption of lithium-ions and electrons, which yields a cross-linked PEO-type polymer. These proposed reactions of the reductive decomposition of FEC can be seen in Figure 9.

The reductive decomposition of many FEC molecules eventually yields the SEI components LiF, Li_2CO_3, $Li_2C_2O_4$, HCO_2Li, and a cross-linked PEO-type polymer as end products. The trapping of cycleable lithium in the SEI by the proposed reductive decomposition of FEC (see Figure 9) is mainly responsible for the capacity loss of the investigated pouch cells with the FEC electrolyte after formation during subsequent cycling. The cross-linked PEO-type polymer shown in Figure 9 is identical to parts of the FEC-derived cross-linked polymer that is proposed by Michan et al.[42] However, a small fraction of the reductively decomposed FEC molecules might react in each case together with one lithium-ion and one electron to form one LiF molecule, one hydrogen atom, and one VC molecule, as described in literature.[56] The formed VC molecules can subsequently react with some of the vinoxyl-radicals to form poly(VC).[56] As a result, some poly(VC) units might also be integrated into the mentioned cross-linked PEO-type polymer. This would explain why minor amounts of poly(VC) are detected

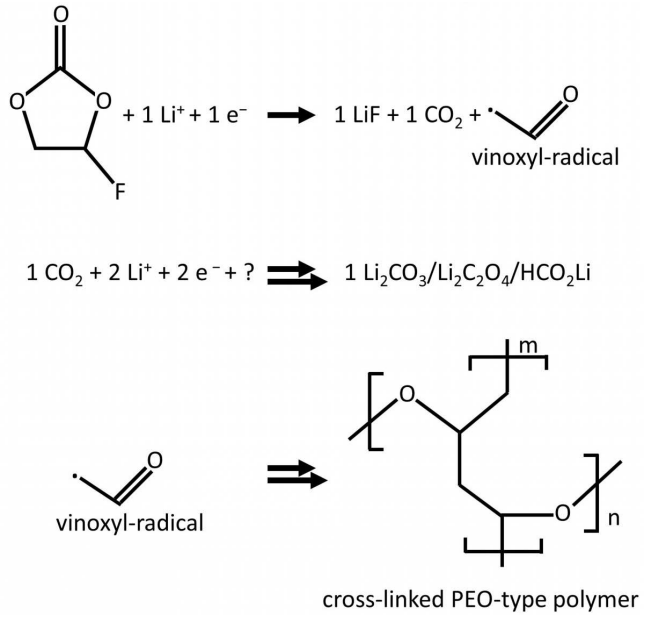

Figure 9. Proposed reactions of the reductive decomposition of FEC. One FEC molecule, one lithium-ion, and one electron react with each other to form one LiF molecule, one CO_2 molecule, and one vinoxyl-radical. The CO_2 molecule, two further lithium-ions, two further electrons, and possibly other molecules react with each other to form one Li_2CO_3 molecule, one $Li_2C_2O_4$ molecule, or one HCO_2Li molecule. The detailed reaction of the CO_2 reduction is unknown. The formed vinoxyl-radicals polymerize with each other yielding a cross-linked PEO-type polymer.

by XPS in the surface layers of the anodes from the cells with the FEC electrolyte after formation and after following cycling. The reactions of the reductive decomposition of VC and FEC (see Figure 8 and Figure 9) are reasonable proposals, but they are not definite. However, we think that these proposals can serve as a base for a further clarification of the reductive decomposition mechanism of VC and FEC in lithium-ion battery cells.

Conclusions

The objective of this study is to gain new information about the reductive decomposition of the electrolyte additives FEC and VC in lithium-ion battery cells. Another related objective is to identify the triggers for capacity loss of pouch cells with silicon-containing anodes during formation and subsequent cycling. For this purpose, NCM622/silicon-graphite lithium-ion pouch cells with two different electrolytes (either 1 M $LiPF_6$ in FEC:DMC or 1 M $LiPF_6$ in VC:DMC) are assembled. Electrolytes, gases, and electrodes from these cells are analyzed before formation, after formation, after 15 cycles, and after 40 cycles. The extracted electrolytes are quantitatively analyzed by HPLC-UV/Vis, HPLC-ESI/MS, and GC-FID to determine the consumptions of the electrolyte components in the cells during formation and subsequent cycling. The cycle data of the investigated cells reveal that the cells with the FEC-containing electrolyte have higher absolute discharge capacities during the first cycles compared to the cells with the VC-containing electrolyte,

whereas the cells with the VC-containing electrolyte have higher capacity retentions compared to the cells with the FEC-containing electrolyte. According to the results from the analyses, the capacity losses of the NCM622/silicon-graphite pouch cells during formation are (almost) exclusively triggered by trapping of cycleable lithium in the SEI and by trapping of cycleable lithium in irreversibly lithiated silicon (Li_xSi_y) and silicon oxide (Li_xSiO_y) under the SEI. After formation during subsequent cycling, the capacity losses of these cells are (almost) exclusively induced by trapping of cycleable lithium in the SEI.

VC is preferentially decomposed during formation and following cycling in the cells with the VC-containing electrolyte. The correlation between the cumulative irreversible capacity and the VC consumption reveals that the reductive decomposition of one VC molecule is associated with the consumption of one electron. It is proposed that the reductive decomposition of one VC molecule at the anode consumes one lithium-ion and one electron. The VC reduction yields a lithium-containing poly(VC), which is the main component of the VC-derived SEI. The relatively high VC consumptions and the relatively low number of consumed lithium-ions per reduced VC molecule explain why the VC-derived SEI is thick and lithium-poor.

FEC is exclusively decomposed during formation and subsequent cycling in the cells with the FEC-containing electrolyte. The correlation between the cumulative irreversible capacity and the FEC consumption shows that the reductive decomposition of one FEC molecule leads to the consumption of three electrons. It is proposed that the reductive decomposition of one FEC molecule at the anode consumes a total of three lithium-ions plus three electrons. The reductive decomposition of FEC yields the SEI components LiF, Li_2CO_3, $Li_2C_2O_4$, HCO_2Li, and a cross-linked PEO-type polymer possibly with some integrated poly(VC) units. The relatively low FEC consumptions and the relatively high number of consumed lithium-ions per reduced FEC molecule are the reasons why the FEC-derived SEI is thin and lithium-rich.

This study demonstrates that the applied method for the determination of the consumptions of the electrolyte components in battery cells can reveal new, valuable information for the clarification of the decomposition mechanisms in battery cells, namely the number of consumed electrons per consumed molecule of the concerning electrolyte component. For future studies, the applied method for the determination of the consumptions of the electrolyte components in battery cells can be used to clarify the mechanisms for the decomposition of further important additives, such as vinyl ethylene carbonate (VEC), ethylene sulfite (ES), 1,3-propane sultone (PS), or lithium bis(oxalate)borate (LiBOB). The clarification of such decomposition mechanisms can contribute to further systematic optimization of lithium-ion batteries.

Acknowledgements

We thank Sven Leuthner for his support in the cell manufacturing. Furthermore, we would like to thank Julian Klemens, Philip Scharfer, and Wilhelm Schabel from Thin Film Technology (TFT) at KIT for the coating of the silicon-graphite electrodes in their TFT Coating and Printing Lab. This work was done at KIT Battery Technology Center (KIT-BATEC) and the XPS work was carried out with the support of the Karlsruhe Nano Micro Facility (KNMFi, http://www.knmf.kit.edu), a Helmholtz Research Infrastructure at KIT. The work contributes to the research performed at the Center for Electrochemical Energy Storage Ulm & Karlsruhe (CELEST). Open Access funding enabled and organized by Projekt DEAL.

Conflict of Interests

The authors declare no conflict of interest.

Data Availability Statement

The data that support the findings of this study are available in the supplementary material of this article.

Keywords: Lithium-ion battery · Silicon-graphite anode · FEC · VC · Pouch cells

[1] M. N. Obrovac, L. Christensen, *Electrochem. Solid-State Lett.* **2004**, *7*, A93.
[2] M. Ashuri, Q. He, L. L. Shaw, *Nanoscale* **2016**, *8*, 74–103.
[3] J. Xu, L. Zhang, Y. Wang, T. Chen, M. Al-Shroofy, Y.-T. Cheng, *ACS Appl. Mater. Interfaces* **2017**, *9*, 3562–3569.
[4] M. Winter, J. O. Besenhard, M. E. Spahr, P. Novák, *Adv. Mater.* **1998**, *10*, 725–763.
[5] M. T. McDowell, S. W. Lee, W. D. Nix, Y. Cui, *Adv. Mater.* **2013**, *25*, 4966–4985.
[6] S. Chae, S. Choi, N. Kim, J. Sung, J. Cho, *Angew. Chem. Int. Ed.* **2020**, *59*, 110–135.
[7] W.-J. Zhang, *J. Power Sources* **2011**, *196*, 13–24.
[8] R. Jung, M. Metzger, D. Haering, S. Solchenbach, C. Marino, N. Tsiouvaras, C. Stinner, H. A. Gasteiger, *J. Electrochem. Soc.* **2016**, *163*, A1705–A1716.
[9] Q. Sun, J. Li, M. Yang, S. Wang, G. Zeng, H. Liu, J. Cheng, D. Li, Y. Wei, P. Si, Y. Tian, L. Ci, *Small* **2023**, *19*, 2300759.
[10] Q. Sun, G. Zeng, X. Xu, J. Li, J. J. Biendicho, S. Wang, Y. Tian, L. Ci, A. Cabot, *Adv. Energy Mater.* **2024**, *14*, 2402048.
[11] T. Jaumann, J. Balach, U. Langklotz, V. Sauchuk, M. Fritsch, A. Michaelis, V. Teltevskij, D. Mikhailova, S. Oswald, M. Klose, G. Stephani, R. Hauser, J. Eckert, L. Giebeler, *Energy Storage Mater.* **2017**, *6*, 26–35.
[12] J. C. Burns, R. Petibon, K. J. Nelson, N. N. Sinha, A. Kassam, B. M. Way, J. R. Dahn, *J. Electrochem. Soc.* **2013**, *160*, A1668–A1674.
[13] S. Solchenbach, M. Wetjen, D. Pritzl, K. U. Schwenke, H. A. Gasteiger, *J. Electrochem. Soc.* **2018**, *165*, A512–A524.
[14] M. Wetjen, D. Pritzl, R. Jung, S. Solchenbach, R. Ghadimi, H. A. Gasteiger, *J. Electrochem. Soc.* **2017**, *164*, A2840–A2852.
[15] L. Chen, K. Wang, X. Xie, J. Xie, *Electrochem. Solid-State Lett.* **2006**, *9*, A512.
[16] N.-S. Choi, K. H. Yew, K. Y. Lee, M. Sung, H. Kim, S.-S. Kim, *J. Power Sources* **2006**, *161*, 1254–1259.
[17] S. Dalavi, P. Guduru, B. L. Lucht, *J. Electrochem. Soc.* **2012**, *159*, A642–A646.
[18] V. Etacheri, O. Haik, Y. Goffer, G. A. Roberts, I. C. Stefan, R. Fasching, D. Aurbach, *Langmuir* **2012**, *28*, 965–976.
[19] Y. Jin, N.-J. H. Kneusels, L. E. Marbella, E. Castillo-Martínez, P. C. M. M. Magusin, R. S. Weatherup, E. Jónsson, T. Liu, S. Paul, C. P. Grey, *J. Am. Chem. Soc.* **2018**, *140*, 9854–9867.
[20] H. Nakai, T. Kubota, A. Kita, A. Kawashima, *J. Electrochem. Soc.* **2011**, *158*, A798–A801.

[21] R. Petibon, V. L. Chevrier, C. P. Aiken, D. S. Hall, S. R. Hyatt, R. Shunmugasundaram, J. R. Dahn, *J. Electrochem. Soc.* **2016**, *163*, A1146–A1156.
[22] R. Stockhausen, A. Hofmann, L. Gehrlein, T. Bergfeldt, M. Müller, H. Ehrenberg, A. Smith, *J. Electrochem. Soc.* **2021**, *168*, 080504.
[23] R. Stockhausen, L. Gehrlein, M. Müller, T. Bergfeldt, A. Hofmann, F. J. Müller, J. Maibach, H. Ehrenberg, A. Smith, *J. Power Sources* **2022**, *543*, 231842.
[24] J. R. Stockhausen, *PhD thesis*, Karlsruhe Institute of Technology, **2023**, DOI: 10.5445/IR/1000158906.
[25] A. Hofmann, A. Smith, F. J. Müller, I.. Reuter, registration number: 22188274.9, **2022**, patent submitted.
[26] K. L. Parry, A. G. Shard, R. D. Short, R. G. White, J. D. Whittle, A. Wright, *Surface Interface Anal.* **2006**, *38*, 1497–1504.
[27] L. El Ouatani, R. Dedryvère, C. Siret, P. Biensan, D. Gonbeau, *J. Electrochem. Soc.* **2009**, *156*, A468.
[28] L. El Ouatani, R. Dedryvère, C. Siret, P. Biensan, S. Reynaud, P. Iratçabal, D. Gonbeau, *J. Electrochem. Soc.* **2009**, *156*, A103.
[29] D. Aurbach, K. Gamolsky, B. Markovsky, Y. Gofer, M. Schmidt, U. Heider, *Electrochim. Acta* **2002**, *47*, 1423–1439.
[30] H. Ota, Y. Sakata, A. Inoue, S. Yamaguchi, *J. Electrochem. Soc.* **2004**, *151*, A1659.
[31] S. A. Delp, O. Borodin, M. Olguin, C. G. Eisner, J. L. Allen, T. R. Jow, *Electrochim. Acta* **2016**, *209*, 498–510.
[32] B. Zhang, M. Metzger, S. Solchenbach, M. Payne, S. Meini, H. A. Gasteiger, A. Garsuch, B. L. Lucht, *J. Phys. Chem. C* **2015**, *119*, 11337–11348.
[33] B. Strehle, S. Solchenbach, M. Metzger, K. U. Schwenke, H. A. Gasteiger, *J. Electrochem. Soc.* **2017**, *164*, A2513–A2526.
[34] K. Leung, S. B. Rempe, M. E. Foster, Y. Ma, J. M. Martinez del la Hoz, N. Sai, P. B. Balbuena, *J. Electrochem. Soc.* **2014**, *161*, A213–A221.
[35] K. U. Schwenke, S. Solchenbach, J. Demeaux, B. L. Lucht, H. A. Gasteiger, *J. Electrochem. Soc.* **2019**, *166*, A2035–A2047.
[36] L. J. Krause, V. L. Chevrier, L. D. Jensen, T. Brandt, *J. Electrochem. Soc.* **2017**, *164*, A2527–A2533.
[37] J. Maibach, F. Lindgren, H. Eriksson, K. Edström, M. Hahlin, *J. Phys. Chem. Lett.* **2016**, *7*, 1775–1780.
[38] X. Zhang, S. Weng, G. Yang, Y. Li, H. Li, D. Su, L. Gu, Z. Wang, X. Wang, L. Chen, *Cell Rep. Phys. Sci.* **2021**, *2*, 100668.
[39] J. Asenbauer, T. Eisenmann, M. Kuenzel, A. Kazzazi, Z. Chen, D. Bresser, *Sustain. Energy Fuels* **2020**, *4*, 5387–5416.
[40] M. A. Al-Maghrabi, J. Suzuki, R. J. Sanderson, V. L. Chevrier, R. A. Dunlap, J. R. Dahn, *J. Electrochem. Soc.* **2013**, *160*, A1587–A1593.
[41] L. Gehrlein, C. Njel, F. Jeschull, J. Maibach, *ACS Appl. Energ. Mater.* **2022**, *5*, 10710–10720.
[42] A. L. Michan, B. S. Parimalam, M. Leskes, R. N. Kerber, T. Yoon, C. P. Grey, B. L. Lucht, *Chem. Mater.* **2016**, *28*, 8149–8159.
[43] E. K. W. Andersson, C. Sångeland, E. Berggren, F. O. L. Johansson, D. Kühn, A. Lindblad, J. Mindemark, M. Hahlin, *J. Mater. Chem. A* **2021**, *9*, 22462–22471.
[44] C. Xu, F. Lindgren, B. Philippe, M. Gorgoi, F. Björefors, K. Edström, T. Gustafsson, *Chem. Mater.* **2015**, *27*, 2591–2599.
[45] X. Chen, X. Li, D. Mei, J. Feng, M. Y. Hu, J. Hu, M. Engelhard, J. Zheng, W. Xu, J. Xiao, J. Liu, J.-G. Zhang, *ChemSusChem* **2014**, *7*, 549–554.
[46] M. Nie, D. P. Abraham, Y. Chen, A. Bose, B. L. Lucht, *J. Phys. Chem. C* **2013**, *117*, 13403–13412.
[47] F. Holtstiege, A. Wilken, M. Winter, T. Placke, *Phys. Chem. Chem. Phys.* **2017**, *19*, 25905–25918.
[48] D. Pritzl, S. Solchenbach, M. Wetjen, H. A. Gasteiger, *J. Electrochem. Soc.* **2017**, *164*, A2625–A2635.
[49] T. Teufl, D. Pritzl, L. Hartmann, S. Solchenbach, M. A. Mendez, H. A. Gasteiger, *J. Electrochem. Soc.* **2023**, *170*, 020531.
[50] M. He, L. Hu, Z. Xue, C. C. Su, P. Redfern, L. A. Curtiss, B. Polzin, A. von Cresce, K. Xu, Z. Zhang, *J. Electrochem. Soc.* **2015**, *162*, A1725–A1729.
[51] R. Petibon, J. Xia, J. C. Burns, J. R. Dahn, *J. Electrochem. Soc.* **2014**, *161*, A1618–A1624.
[52] F. A. Soto, Y. Ma, J. M. Martinez de la Hoz, J. M. Seminario, P. B. Balbuena, *Chem. Mater.* **2015**, *27*, 7990–8000.
[53] D. Kuai, P. B. Balbuena, *ACS Appl. Mater. Interfaces* **2022**, *14*, 2817–2824.
[54] K. Schroder, J. Alvarado, T. A. Yersak, J. Li, N. Dudney, L. J. Webb, Y. S. Meng, K. J. Stevenson, *Chem. Mater.* **2015**, *27*, 5531–5542.
[55] I. A. Shkrob, J. F. Wishart, D. P. Abraham, *J. Phys. Chem. C* **2015**, *119*, 14954–14964.
[56] Y. Jin, N.-J. H. Kneusels, P. C. M. M. Magusin, G. Kim, E. Castillo-Martínez, L. E. Marbella, R. N. Kerber, D. J. Howe, S. Paul, T. Liu, C. P. Grey, *J. Am. Chem. Soc.* **2017**, *139*, 14992–15004.